

# Extracting the shear wave velocity structure of deep alluviums of “Qom” Basin (Iran) employing HVSR inversion of microtremor recordings

Shahram Maghami <sup>a</sup>, Abdollah Sohrabi-Bidar <sup>a,\*</sup>, Samuel Bignardi <sup>b,e</sup>, Ahmad Zarean <sup>c</sup>, Mohsen Kamalian <sup>d</sup>

<sup>a</sup> School of Geology, College of Sciences, University of Tehran, Tehran, Iran

<sup>b</sup> School of Electrical and Computer Engineering, Georgia Institute of Technology, Atlanta, GA, USA

<sup>c</sup> Department of Civil Engineering, Shabestar Branch, Islamic Azad University, Shabestar, Iran

<sup>d</sup> Geotechnical Engineering Research Centre, International Institute of Earthquake Engineering and Seismology (IIEES), Tehran, Iran

<sup>e</sup> Interuniversity Center for 3D Seismotectonics with territorial applications, CRUST-UniFE, Ferrara, Italy

## ARTICLE INFO

### Article history:

Received 5 February 2020

Received in revised form 21 November 2020

Accepted 18 December 2020

Available online 9 January 2021

### Keywords:

Qom Basin

Microtremor

Inversion

HVSR

Subsurface structure

## ABSTRACT

In recent decades, numerous observations of the connection between sedimentary basins structure and severity and variability of damages during earthquake events have sparked a series of studies for characterization of such subsurface structures. However, these investigations were always accompanied with cost concerns and executive restrictions. Among non-destructive and cost effective approaches which have been developed in seismic response evaluations, usage of microtremor has attracted considerable attentions. In the current study, we have focused on inversion of microtremor acquired in the Qom basin, Iran. As the area is known to be seismically active, our main contribution is the construction of a three-dimensional model of the sedimentary basin in terms of shear wave velocity, which extends and integrates the previous knowledge (limited to the Vs30) down to the bedrock. Additionally, we provided further evidence of several possible faults in the area, one of which has been introduced earlier but poorly investigated so far: the “Qomrud” Fault. The results of a series of previous studies on the area, comprising down-hole surveys, electrical resistivity surveys, surface seismic refractions and surficial bore-hole excavations have been used, either to form a more precise initial model for inversion process or to evaluate the outputs. Additionally, we investigated possibility of obtaining the distribution of the Vs30 in the area directly from inversion of HVSR curves. It revealed that, although for relatively shallow bedrocks (80–100 m) the differences of achieved velocities is lower than 10–15%, in deep sediments, the Vs30 from microtremor is largely overestimated. Furthermore, we discussed the applicability of empirical relationships for estimating bed-rock depth in the investigated basin.

© 2020 Elsevier B.V. All rights reserved.

## 1. Introduction

In the context of sedimentary basins, the interrelationship between dynamic properties of sediments and seismic response at the surface is nowadays well understood. It is well known that presence of a sedimentary cover may result in large amplifications of the seismic motion and high damage even for moderately weak earthquakes. In addition, amplification may present wide local variations across the affected area. Investigating the seismic response of such, potentially wide, areas by leveraging direct sampling (e.g. bore-hole, excavations, and other geotechnical investigations), is often prohibitively costly, and despite the fact that costs may be lowered by leveraging geophysics, most methods are difficult to deploy when urban areas are concerned.

To overcome these limitations, Kanai et al., (1954) investigated the application of microtremors in seismic studies. Subsequently,

Nakamura, (1989) developed the well-known Horizontal to Vertical Spectral Ratio (HVSR or H/V), which proved to be an extremely cost-effective and rapid tool for seismological investigations, and particularly well suited to study extensive areas (e.g. Nakamura 1989; Nakamura 2019).

Recent introduction of new low-cost and portable sensors and advancement in numerical modeling and inversion techniques, largely popularized the HVSR method and improved our capability of investigating large areas and gain a better understanding of their seismic behaviour. Since its introduction, HVSR has been applied in an increasing number of studies worldwide, to determine the fundamental vibration frequency of the sedimentary cover. For example, in the studies of the Grenoble basin (Cornou et al. 2008), Thessaloniki basin (Raptakis and Makra 2010), Trabzon-Arsin Basin (Akin and Sayil 2016), the horizontal to vertical spectral ratio, as computed in the HVSR method, was leveraged to explore the seismic response of the sites in frequency domain and assess the resonance frequency(ies) of the sediments. The application of HVSR from ambient noises has also been employed in geotechnical

\* Corresponding author.

E-mail address: [asohrabi@ut.ac.ir](mailto:asohrabi@ut.ac.ir) (A. Sohrabi-Bidar).

applications to obtain 1D (i.e. layered) shear wave velocity profiles (Raptakis and Makra 2010).

It was shown that the reliability of such S-wave velocity structures is sufficient to justify the application of the HVSR method in seismic hazard analysis (Fäh et al. 2003).

The composition of the wavefield, in terms of wave propagation modalities (P, S, Surface Waves, etc.) contributing to the formation of the spectral peaks and to the general shape of the HVSR curve, may depend on many factors, but there is common agreement on the fact that the peak(s) occur at the resonance frequencies of Vs waves. This has led to different modeling approaches. For example, Tsai and Housner (1970) consider the HVSR as the result of sub vertically propagating body wave, while Lunedei and Albarello (2010) tend to associate the HVSR with the dispersion curves of surface waves. This has also influenced the inversion of such data and attempts to enrich the HVSR with a-priori information and leverage the joint inversion of HVSR and surface waves are becoming increasingly common. In order to improve the reliability of the velocity structure of the basin, down to the bedrock, Moon et al., (2019) considered both array measurements and single station HVSR. They emphasized that, among the four interpretation approaches they tested, namely bilinear intersection method, preselected Vs based approach, normalized phase velocity approach, and HVSR analysis, the latter provided the best estimation for the bedrock depth. This is interesting, especially considering the operational simplicity of HVSR compared to other methods.

Arai and Tokimatsu, (2005) applied a joint inversion scheme to four study sites and compared the achieved shear wave velocity structure down to the bedrock with conventional inversion techniques. They showed that joint inversion can produce results more consistent with available down-hole velocity logs, as compared to the same techniques used independently. Gouveia et al., (2019) also emphasized on better velocity estimation of joint inversions for deeper parts.

Summarizing, HVSR successfully be employed in joint inversion, where it provides a valuable constraint on the depth of bedrock. Conversely, the inversion of HVSR curves per-se is improved if a-priori information, such as thickness of layers or the range of shear wave velocity, is provided to the inversion (Fäh et al. 2003).

In addition, it is worth of note that obtaining the VS30 parameter from inversion of microtremor has also been investigated. Zor et al., (2010) leveraged inversion of single station microtremor measurements to generate a Vs30-based site classification map and to retrieve information on sediment-bedrock structure of the Izmit Bay area (Turkey). Özalaybey et al., (2011) further investigated the Izmit Bay basin with focus on its 3D structures and site response. While doing so, they combined single station microtremor and gravity measurements to produce a resonance frequency map of the area. Moreover, Pamuk et al., (2017) evaluated the Izmir bay basin depth using a combination of microgravity method and microtremor recordings. Rahman et al., (2016) used microtremor measurements along with downhole seismic and standard penetration test to characterize shear wave velocity of near surface materials In Chittagong City (Bangladesh).

Many researches highlighted how integrating geophysical and geological investigations allows reconstructing detailed and valuable subsurface models for seismic hazard and risk assessment (Panzera et al. 2019), for example, Pilz et al., (2010), leveraged the inversion of HVSR curves from 125 single-station acquisitions to determine the S-wave velocity structure of the basin of Santiago de Chile. To do so, they constrained the thickness of the sedimentary cover using estimates from gravimetry. The obtained Vs30 showed good correspondence with local geology. Distribution of the intensities for the 1985 Valparaiso event also pointed out that high intensities were consistent with local low VS30 values and thick sedimentary cover. Moreover, Akkaya and Özvan (2019), utilized several geotechnical and geophysical measurement including borehole excavations, seismic profiling, multi-channel

analysis of surface waves (MASW) in combination with microtremor to determine properties of sediments in Van area (Turkey) obtaining good agreement between soil type and amplification frequency of the sediments.

Mahajan et al., (2012), conducted active (MASW) and passive (HVSR) investigations at 30 sites in the frontal part of the Himalaya, which is characterized by soft sediments and strong seismological effects. They emphasized on the application of both techniques in site effect characterizations. Cipta et al., (2020) inverted microtremor HVSR curves obtained prior to a M 7.8 earthquake, for unearthing a fault which ruptured about 180 km after the earthquake. It is revealed that the HVSR inversion was able to locate subsurface fault crossing the city and its dipping direction. Moreover, the systematic damage distribution in the area was shown to correlate with VS structure of the sediments obtained from microtremor inversion. Bekler et al., (2019) Have performed seismic microzonation for the city of Çanakkale, in northwest of Turkey. To that end, an integrated geophysical and geo-technical study was performed in a detailed manner including MASW and microtremor measurements. Tün et al., (2016), have extracted bedrock depth and shear wave velocity structure of Eskişehir Basin in Turkey with the aid of single station and array microtremor data, seismic reflection data, and shallow and deep borehole drillings.

Sauret et al., (2015), characterized superficial deposits using a combination of electrical resistivity tomography and horizontal to vertical spectral ratio in the Kou basin in Burkina Faso (West Africa), and mapped the bedrock as well as basin sediments highlighting the role of faulting and magmatic intrusion in the basin formation. They emphasized on the efficiency of the combined use of ERT and HVSR as complementary sources of information for the characterization of superficial deposits.

Despite modeling of microtremors in realistically full 3D structures taking into account all propagation modalities, is still far beyond reach, recent numerical methods allow to leverage HVSR to efficiently investigate large areas in terms of subsurface shear wave velocity and depth and morphology of bedrock (Wathelet et al. 2004; Herak 2008; Bignardi et al. 2018). Although the most advanced inversion algorithms have proven reliable for subsurface characterization, these methods are often overcomplicated for the general purpose of evaluating the bedrock depth. In fact, over the years several empirical relationships have been introduced to tackle this specific task. Such approaches propose a correlation between the frequency of microtremor determined to be the fundamental mode and depth of the bedrock (e.g. Ibs-Von Seht and Wohlenberg 1999).

In the present study, we investigate the Qom sedimentary basin (Iran) by means of 43 single station microtremor measurements collected across the area. The horizontal to vertical spectral ratios of these recordings have been inverted in order to investigate the shear wave velocity structure of the sediments. The results from three deep down-hole surveys performed in the region have been used as a primary reference to define a realistic initial model for the microtremor inversions. Moreover, a characteristic depth contrast has been established in the initial model according to the findings of several electrical resistivity surveys performed in the studied area. The local one-dimensional shear wave velocity profiles obtained by inversion of the 43 HVSR curves have been combined to produce a three-dimensional model capable of conveying the main structural aspects of the subsurface. Additionally, to better highlight the lateral variation of the model, several two-dimensional profiles perpendicular to the basin elongation have been extracted. Finally, we compared the velocities of the shallow 30 m, obtained from HVSR, with the analogous result obtained from a set of 34 surface seismic refraction surveys and for deeper sediments, with the results of 3 down-hole surveys. In the following, geographical and geological aspects of the investigated area will be described in section 2. Section 3 is devoted to the description of the geophysical investigations that contributed to the construction of a model for the initialization of the HVSR inversion (down-hole surveys, electrical

resistivity surveys, surface seismic refraction surveys and microtremor recordings) as well as the description of the microtremor survey. Finally, section 4 discusses the inversion methodology, and the three-dimensional Vs model achieved for the Qom basin. The latter will be described through aerial maps, 2D profiles and 3D illustrations. In particular, we will highlight few anomalies that in our perspective are associated with rock faults. Finally, we will comment on the comparison of Vs30 as obtained from HVSR inversion and in-well measurements. In addition, to evaluate the reliability empirical relations in estimating the thickness of sediments at the Qom basin, in the discussion section we will compare the depth of the bedrock achieved from HVSR inversion and the depth obtained from empirical relations commonly encountered in the literature. Conclusion will follow. All artwork in this paper is available online. Interested reader are encouraged to visit the at the url: [https://qgiscloud.com/ShahramMaghami/Qom\\_SurveyLocations\\_8\\_2/](https://qgiscloud.com/ShahramMaghami/Qom_SurveyLocations_8_2/).

## 2. Description of the investigated area

Qom city is located at the northern margin of central Iran, 120 km south of Tehran. The city covers an area of approximately 180 km<sup>2</sup>. This region has witnessed a moderate seismic activity in the past 50 years, including more than 20 earthquakes with magnitudes greater than 4, on the Richter scale. For example, Salafchegan 1960 ( $M_b = 5.1$ ) and 1971 ( $M_b = 5.5$ ) earthquakes, with epicenters located nearly 35 km south of Qom city. Kamalian et al., (2008) estimated 475 years return periods and PGA exceeding 0.6 g for some parts of the city. Extensive geotechnical investigations carried out at this basin by the Qom Water

Resources Company (QWR 2009) suggest the presence of deep alluviums beneath the city, with thickness exceeding 280 m in some areas. The shallow subsurface, down to 20 m depth, mainly consists of cohesive soil layers, followed by granular non-cohesive sediments (20 to 40 m). The deeper subsurface consists of consolidated sediments with shear wave velocities higher than 750 m/s, acting as seismic bedrock. The basin has a north-west to south-east trend which, similarly to most geological structures in the area, is parallel to the Zagros mountain range. Additionally, the southern parts of the city are characterized by sharp elevated cliffs, with NW-SE elongation (Fig. 1), formed by the dominantly massive limestone of the Qom Formation. Fig. 1 presents geological map of the investigated area and locations of earthquakes occurred in the last 50 years.

## 3. Geophysical investigations

While the present paper mainly focuses on microtremor, the present result leveraged information from a wider set of methods. In the following, such geophysical investigations will be outlined in four different sections, one for each methodology. Most of these surveys were performed as a part of underground water exploration studies in Qom basin by the Qom Water Resources (QWR) company and from seismic hazard microzonation studies performed by the International Institute of Earthquake Engineering and Seismology of Iran (IIIES 2005). Data from these sources has been interpreted and leveraged both to increase the accuracy of inputs and to evaluate the reliability of the result obtained from the inversion of microtremor. In particular, we obtained an estimation of the

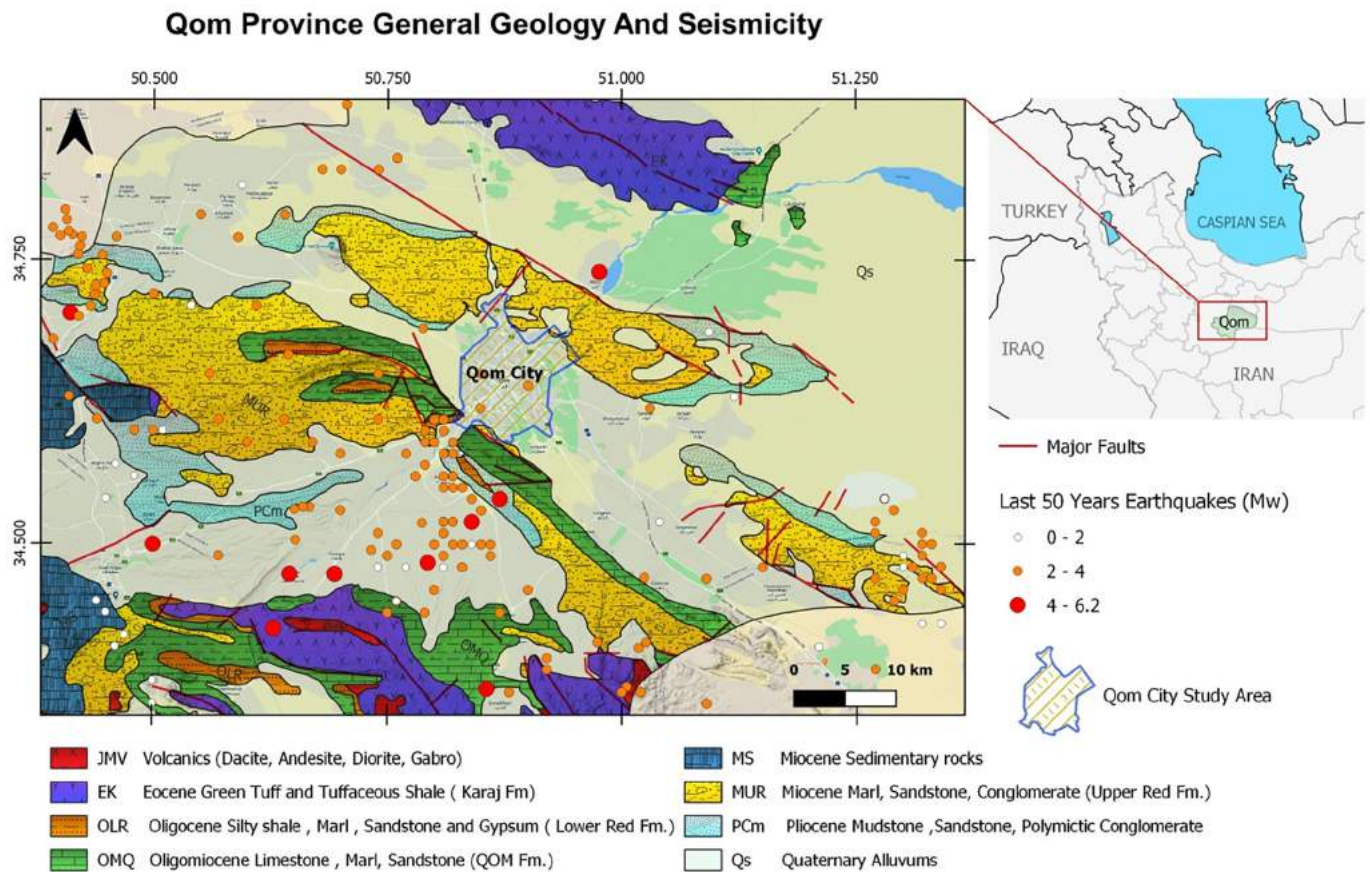


Fig. 1. Simplified geological map of Qom area and distribution of earthquakes occurred in the last 50 years.

sedimentary cover thickness from an electrical resistivity survey (QWR., 2009), and an estimation of the average shear wave velocity in the shallowest 30 m ( $V_{s30}$ ) from seismic refraction (IIIES 2005). Also, down-holes available in the area provided additional information to benchmark our models. In the following, we provide an overview of our information sources. Nevertheless, interested readers may submit an official release request for reports QWR (2009) and IIIES (2005) or refer to the article from Kamalian et al., (2008).

### 3.1. Down-hole surveys

Three down-hole surveys were performed at the locations DH1, DH2 and DH3 in Fig. 2. The seismic source consisted of a sledgehammer hit at the surface, at 3 m of distance from the borehole. Compressional (P) and

shear (S) waves were generated through vertical hit on a plate and horizontal hit on a metallic table, respectively. Three-component geophones placed at increasing depths (step 2 m) were used to record the propagating waves. The length of recorded traces was set to 1 s with 2 millisecond sampling. The direct investigation reached a depth of 100 m for both DH1 and DH2, and 50 m for DH3, and provided the velocity profiles shown in Fig. 2. In DH1, four layers can be observed. The shallowest soil (3 m) possesses S-wave velocities below 150 m/s. Shear wave velocity remains limited (460 to 550 m/s) to a depth of approximately 42 m, where it doubles due to a sudden change in lithology. The second borehole, DH2, evidences 7 major layers. The first three, within the shallow 10 m with S-wave velocities up to 300 m/s. A layer with S-wave velocity about 650 m/s connects the shallow low velocity section to the next three high velocity layers, which all possess shear

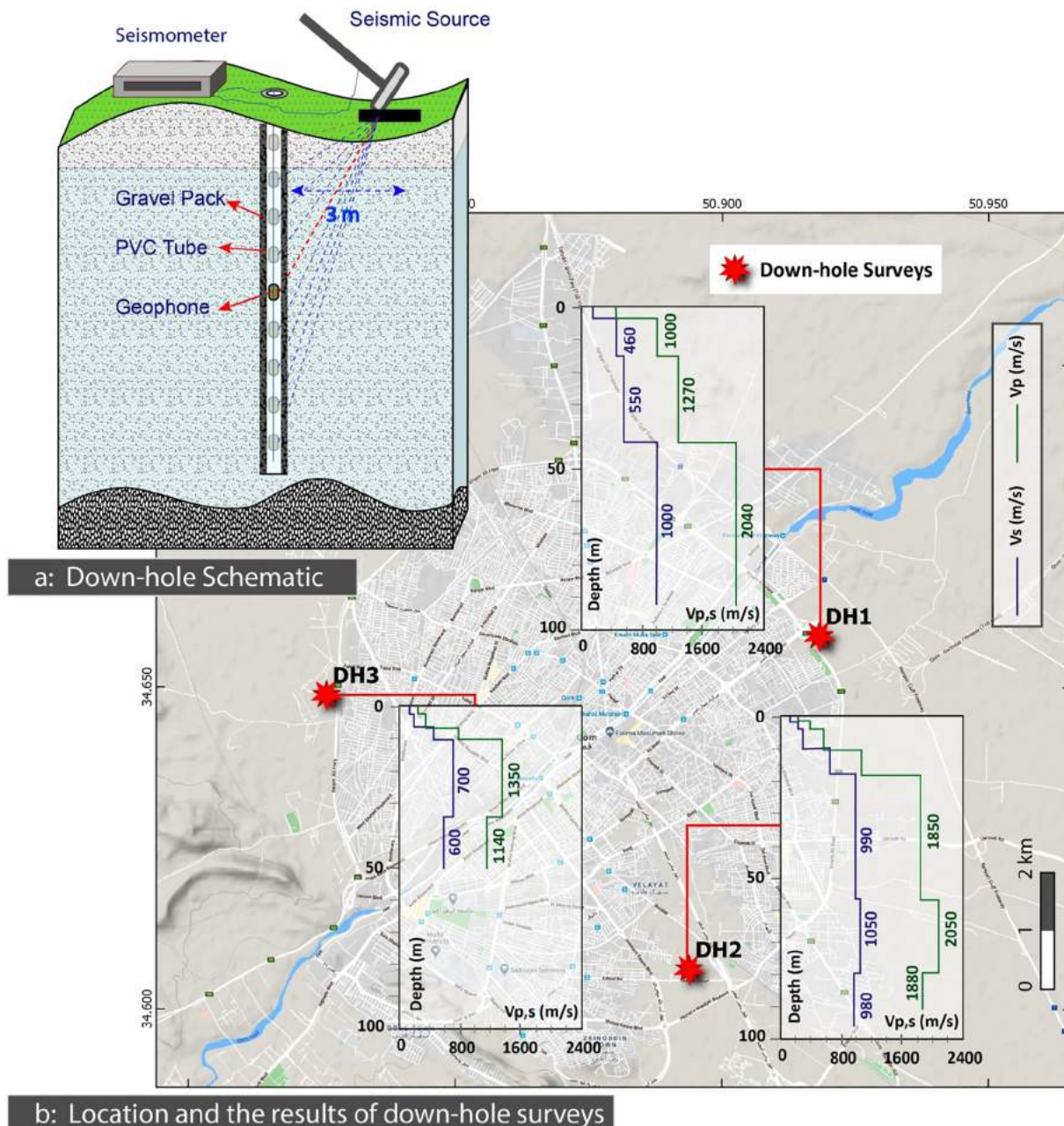


Fig. 2. a) Schematic of down-hole surveys and b) Velocity with respect to depth, as obtained from three shown boreholes.  $V_p$  and  $V_s$  are shown in green and blue, respectively.

wave velocities around 1000 m/s. In the third Borehole, DH3, the top three layers (within 10 m depth) show Vs up to 450 m/s, while in the next 40 m, the Vs increases to 600–700 m/s.

### 3.2. Electrical resistivity surveys

The Qom city is located on an almost NW-SE elongated sedimentary basin with bedrock outcrops especially evident in the southern part of the city. Therefore, in order to cover the most area of the basin, the QWR Company (2009) carried out several deep vertical electrical soundings of variable length along this geometrical trend. Symmetrical Schlumberger electrode array with maximum electrode spacing of 1000 m were employed. This configuration enabled investigating the structure of the alluviums down to about 250–300 m. In each profile, different number of vertical electrical soundings is considered according to the length of the profile. In order to produce a map of the sediments deep structure (i.e. electrical resistivity contrasts), we extracted from this extensive data

set 10 profiles which locations overlaps our investigated area. Fig. 3 shows the results as isothickness map along with some of vertical soundings profiles. These data which presents the deepest resistivity contrast in the VES results, have been used to produce a characteristic constrain to our initialization models to the HVSR inversion, so to limit the range of variations of thicknesses under the assumption that the change in electric parameters corresponds to a change in elastic characteristics as well. Section 4 will discuss the methodology.

### 3.3. Surface seismic refraction

In 2005, in order investigate the shallow structure of the area, 33 surface seismic refraction surveys were performed (IIEES-Report, 2005). The field setup consisted of 24 geophone arranged in a linear array with 4 m spacing. The seismic source was a sledgehammer hit performed in-line with the array, at five different offsets, 4 and 12 m before the first geophone, 5 and 15 m after the last geophone, and

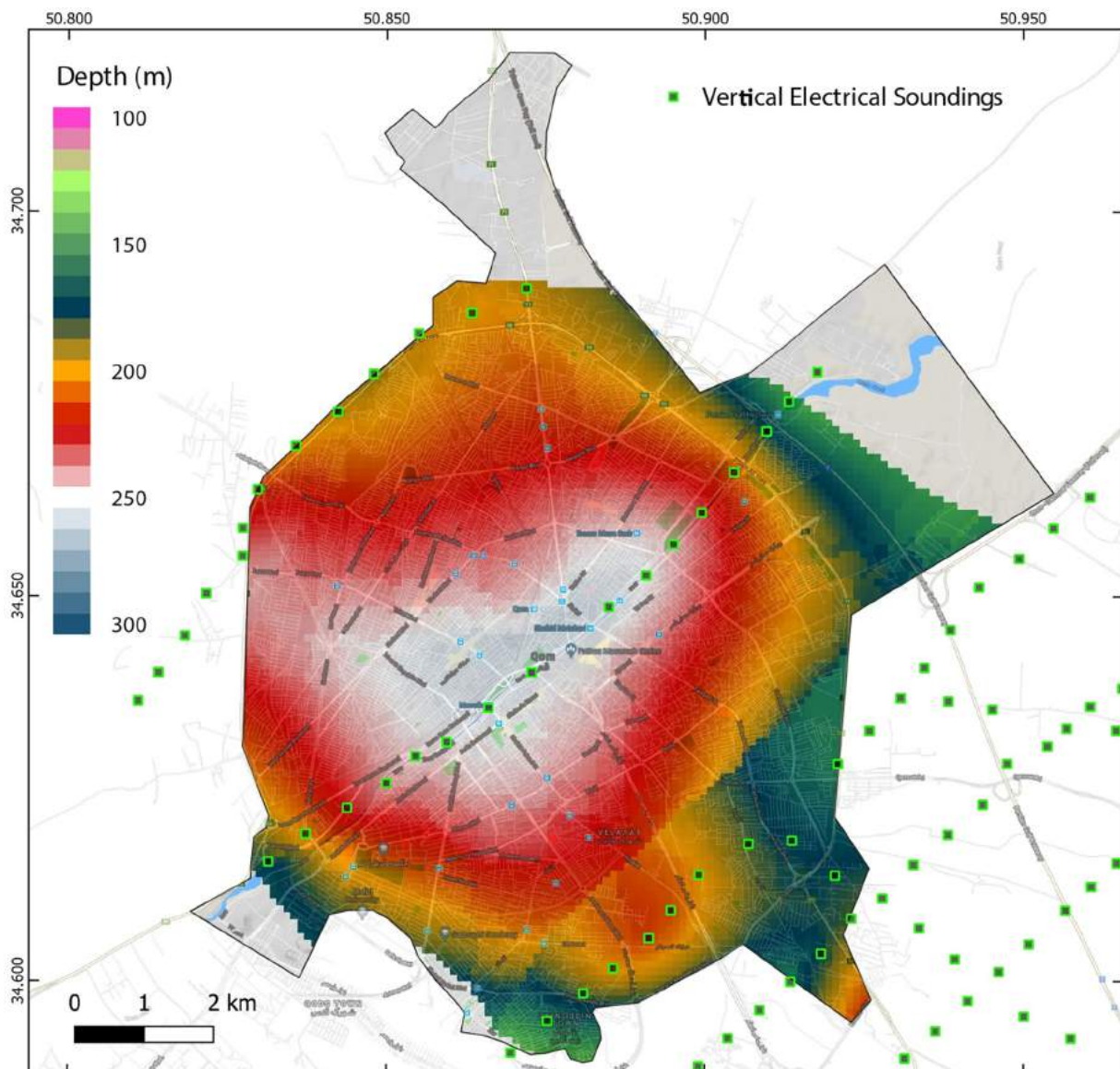


Fig. 3. Map representing the depth of the deepest resistivity contrast as obtained through an extensive electrical resistivity survey performed by the QWR Company (QWR, 2009).

additional hits between geophones number 12 and number 13. Sampling rate and recording duration were set to 2 milliseconds and 1.6 s, respectively. Both P and S waves were considered. Compressional waves were generated through a vertical hit on a plate, while shear waves were produced by horizontal hit on a metallic table. Further details on field operations and data analysis can be found in the IIEES-Report (2005).

The maximum investigation depth of the seismic refraction method is mostly limited by the penetration of the energy released by the seismic source. Since the sledgehammer is considered of the low-energy kind, the investigation depth was limited to 30 m. Therefore, in order to characterize the Vs30, essential for evaluating the dynamic properties of soil, the results from geotechnical investigations in 150 surficial boreholes, including SPT (standard penetration test) were used to enhance the result from the seismic refraction and to construct representative structural grids of the surficial sediments all across the investigated area. Such information, previously published in Kamalian et al., (2008) and shown in Fig. 4 in terms of distribution of the Vs30 across the area

of interest was used in this research both to initialize the shallow portion of the HVSR inversion model and later to evaluate to what extent Vs30 could be retrieved from HVSR inversion alone.

### 3.4. Microtremor recordings

The microtremor survey represents the central part of this article. The main contribution provided here is new insight into the local Vs and its lateral variation, especially for depths that were not yet investigated (i.e. beyond 30 m and down to bedrock). Additionally, we aim at gaining an insight of the bedrock's morphology. To do so, 43 single-station microtremor measurements were acquired across the area (Fig. 5). Three components of ambient noises have been recorded for at least 30 min at each station using a Guralp 6TD broadband weak motion seismometer (velocity meter). Microtremor data have been processed using the standard HVSR procedure (Nakamura 1989; SESAME, 2004). The HVSR curve was computed for each record, using 30s windows with 25% overlap. Smoothing type of Konno and

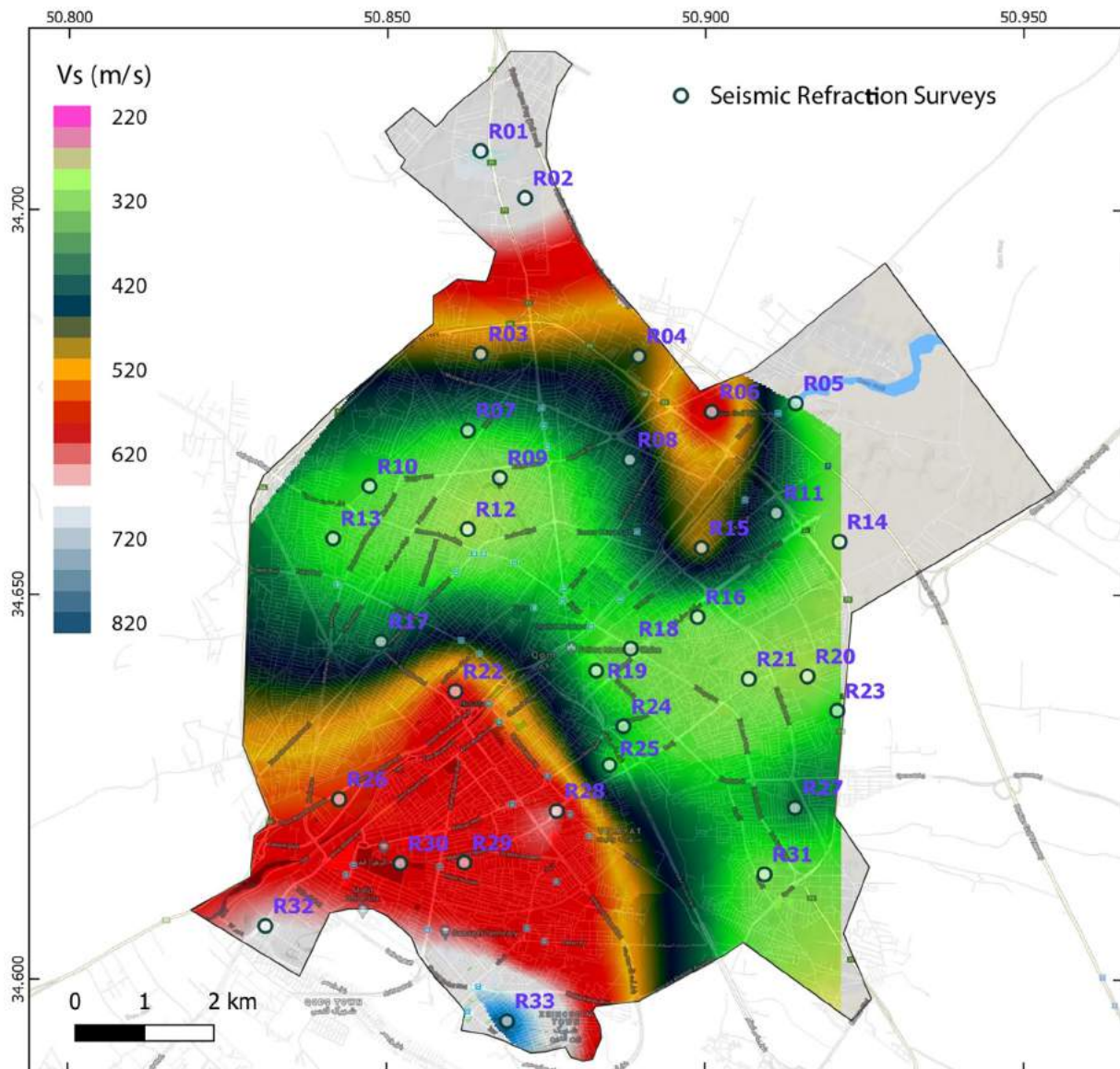


Fig. 4. Distribution of the average shear wave velocities of the shallow 30 m (Vs30) obtained from seismic refraction and other geotechnical investigations including SPT (IIEES-Report, 2005). S-wave velocity increments are illustrated in color.

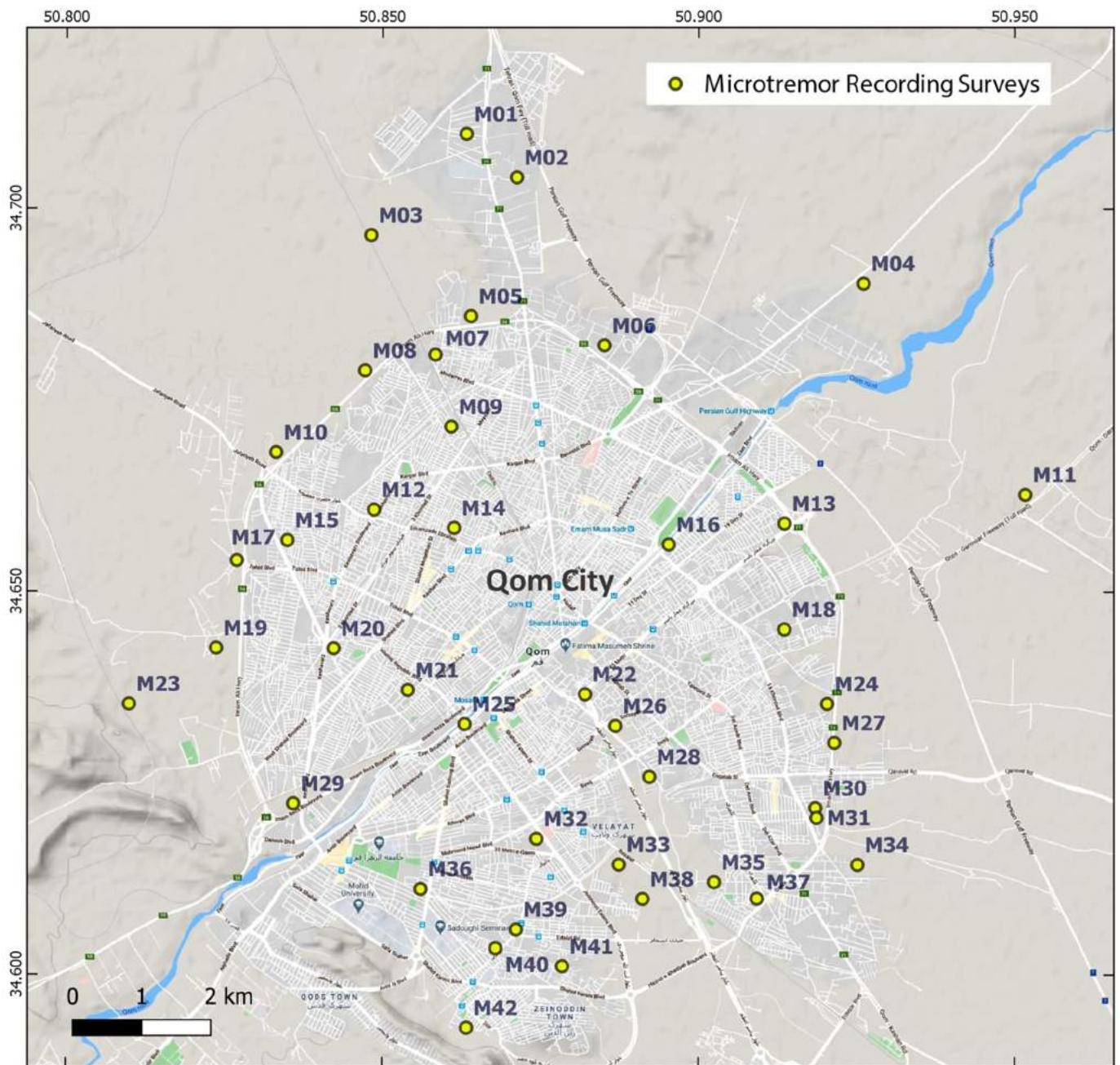


Fig. 5. The location of microtremor recording sites in Qom city.

Ohmachi (1998) with smoothing constant of 40.0 is considered. Additionally, baseline correction and band-pass filtering between 0.1 and 30 Hz were applied.

Almost all stations located on the alluviums show a frequency peak below 1 Hz and many others show an additional peak at about 10 Hz. Sesame (2004), define the criteria for the identification of a “reliable peak” and describe how such a peak is related to the soil’s fundamental resonant frequency.

#### 4. Extracting the S-wave velocity structure

The shape of the HVSR curve may be affected by many factors: presence of wind during the acquisition (Mucciarelli et al. 2005), topography (Chávez-García et al., 1997), presence of nearby elevated

structures (Gallipoli et al. 2013), subsurface lateral variations (Bignardi et al. 2013, 2017), and nature of the wavefield being observed (Bonney-Claudet et al. 2008).

The relative contribution of different seismic phases (P, S, Surface waves, etc.) to the ambient vibration is, indeed, a still a debated topic. The key and controversial aspect is the relative contribution of body and surface waves (Lunedei and Malischewsky 2015). Despite it is quite understood that the HVSR curve will, in general, present local maxima at the resonance frequencies of the S waves regardless of the nature of the wavefield (Albarello and Castellaro 2011), such a controversy has led to the development of inversion algorithms based on different assumptions. On the one hand, as Nakamura recently explained (Nakamura 2019), the origin of the peak of the HVSR at its predominant frequency ( $F_0$ ), can be explained in terms of multiple reflection of SH

waves. In the context discussed by Nakamura (2019) contribution to the wavefield from surface waves is included, but the energy of Rayleigh waves is small around the frequency  $F_0$ . Accordingly, Herak (2008) and Herak et al., (2010) proposed a Montecarlo inversion based on the modeling algorithm proposed by Tsai and Housner (1970). The latter computes the HVSR curve under the assumption that the peak is generated by sub-vertically propagating P and S waves.

On the other hand, several authors assumed the propagation of surface waves as the central contribution to ambient noise. As such, they compare the HVSR curve with the dispersion curve of the fundamental mode of Rayleigh wave (e.g. Konno and Ohmachi 1998; Wathelet et al. 2004). For example, Lunedei and Albarello (2010) investigated a statistical approach to surface waves in their modeling efforts. Noteworthy, the routine from Lunedei and Albarello (2010) was actually available in Herak (2008) as well, but used only for comparison purposes.

Herein, the HVSR curves obtained for 43 stations have been inverted using the software "OpenHVSR-Inversion", an interactive toolbox written in Matlab<sup>®</sup>, designed for the simultaneous modeling and inversion of large Horizontal-to-Vertical Spectral Ratio datasets, specifically designed to construct 2D/3D subsurface models (Bignardi et al. 2016). This software comprises both the formulations from Tsai and Housner (1970) and from Lunedei and Albarello (2010). Additionally, OpenHVSR implements a very interactive graphical interface which privileges flexibility of use and tools for reusing the result obtained at one location as a starting model for locations possessing a similar HVSR curve. As a result, the whole inversion process is considerably speeded up. The interested reader may refer to (Bignardi et al. 2016, 2018) for details on the implementation, methodology and tools included in the OpenHVSR software.

OpenHVSR requires the user to provide an initial model, which includes thicknesses and visco-elastic properties of the subsurface layers under the locations at which measurements were performed. The inversion process will then optimize such parameters. It is assumed that the bottom layer of the model (for which no thickness is required) represents the bedrock. Accordingly, in this study, we leveraged the geophysical resistivity surveys and down-hole surveys to produce the necessary initial model. The bedrock depth was individuated using the results from the resistivity survey by selecting the deepest significant resistivity contrast. However, this depth is allowed to be changed during the inversion process. Additionally, results from down-hole surveys were used to constrain the upper part of the model and to define four sedimentary layers with increasing S-wave velocity.

The remaining parameters required for the inversion process consist of compressional wave velocity and density of the alluviums. Considering the low sensitivity of the shape of the HVSR curve with respect to the compressional wave velocity ( $V_p$ ), this parameter was simply assumed to be equal to twice the shear wave velocity. This seemed an acceptable assumption, especially because it is also consistent with the result from the down holes. Regarding density, information from additional 50 surficial boreholes with depths up to 25 m was considered (IIEES Report, 2005). Density values for deeper layers were constructed starting from the value at the top of sediments and introducing an increasing trend with depth, to account for the increasing compaction. As such, density ranged from 1.6 g/cm<sup>3</sup> for the surficial layer to at most 2.5 g/cm<sup>3</sup> at bedrock. However, the density parameter has the lowest impact on the shape of the HVSR curves (Wathelet et al. 2004; Bignardi et al. 2016;). Additionally, while some of our choices might seem arbitrary, this model is only meant to provide a credible and realistic input to facilitate the inversion. The inversion algorithm will then optimize the subsurface parameters and provide a results that is ideally independent from such initialization.

#### 4.1. Methodology

The methodology we adopted is based on starting the inversion from minimal subsurface models and add progressively new layers. In this study the inversion process has been performed in two phases. In the first (I), the above mentioned initial model has been used for inversion in the low frequency band, i.e. 0.3 to 3.0 Hz. In fact, low frequencies are expected to be more affected by deep layers when compared to the higher part of the spectrum. Subsequently, the output models of phase I have been used as initial models for phase II, this time for the inversion of the full frequency range of interest (0.3 to 30.0 Hz). In phase II thickness and velocities of deepest layers were kept fixed. It is worth of note, however, that in few cases, it was necessary to relax, to some extent, the constrain to the deepest layers, especially when a considerably higher velocity layer was suggested by inversion in the upper portion of the model. Moreover, during the second phase, two additional layers have been added to the shallow portion of the subsurface model with respect to the geometry used in the first phase of inversion. In fact, by allowing additional degrees of freedom in the model, the effects at high frequency generated by the shallow subsurface were better reproduced. To provide a clearer description of this methodology, four examples of the inversion models have been presented in Fig. 6. These models are related to the stations M05, M21 and M22, M39 (Fig. 5). Similar images for the complete set of microtremor measurements are available in the appendices (Fig. A-1). The dotted blue line indicates the initial model (beginning of phase I), in which, the depth achieved by electrical resistivity surveys and four layers have been estimated with equally increasing velocities in the range suggested by the down-hole surveys. The black solid line shows the results after the first inversion phase. Noteworthy, a thick layer with velocities about 1000 m/s can be observed, which presence is in good accordance with downhole surveys. Almost similar conditions can be observed at all the studied locations. The black line model also represented the initial model for the inversion phase II. Nevertheless, each of the two surficial layers was split in two, yielding four layers in the shallow portion of the model. The deepest layer has been kept fixed both in terms of thickness and velocities. However, since the thickness of surficial layers was allowed to change, its actual depth was free to change as well. The dashed red line illustrates the results of the second phase of inversion. Results will be discussed in following sections. Fig. 7 shows the HVSR obtained for the same four selected stations M05, M21, M22 and M39 (dashed red line) and the HVSR of the lowest misfit models for both phases of inversion (solid blue for phase I and large dashed green line for phase II). Similar results for the whole set of measurement stations have been presented in appendices (Fig. A-2:). As highlighted before, two major peaks are evident in most the stations; one at about 1.0 and a second at about 10 Hz.

As it is common in every inversion approach, the first performance indicator for a successful inversion is the minimization of the so-called "energy functional", sometime referred as "misfit". In the present case, the misfit measures the squared difference between the spectral ratios obtained from the data and the simulated HVSR curves. To achieve such minimization, the guided Montecarlo algorithm was set to perform 25,000 iterations for each location in the survey, and during both phase I and phase II.

Since the initial misfit is variable across different locations, it is usually more informative to normalize it with respect its initial value. As such, the normalized misfit, is a curve that starts at one and is monotonically decreasing with iterations. In the first inversion phase (for the low frequency range), the misfit was reduced to values lower than 0.1 for 32 stations, it ranged between 0.1 and 0.2 for 7 stations, and remained above 0.2 for the remaining 4. Phase II, although exploiting an already optimized model includes a larger amount of data and represents a

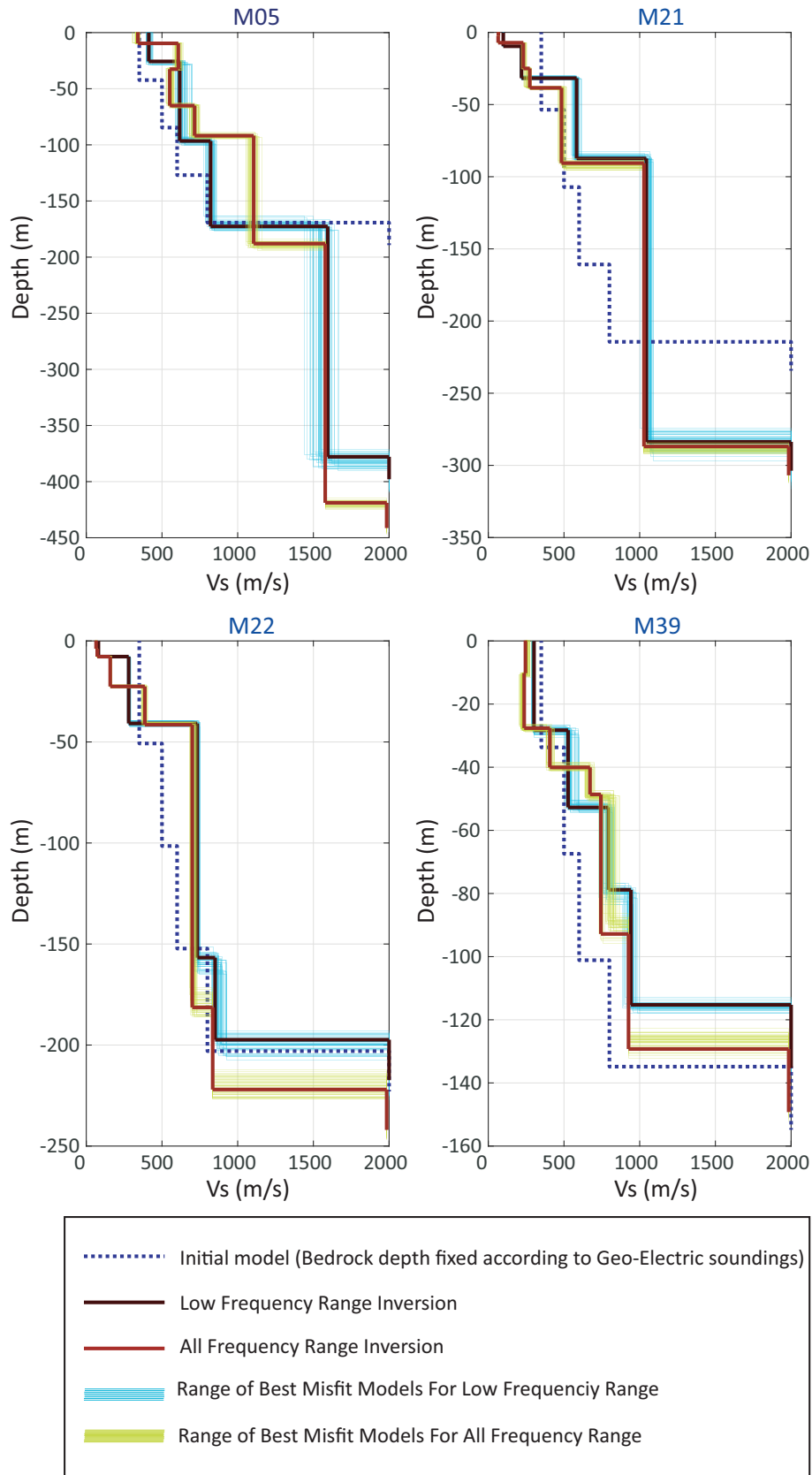


**Fig. 6.** Examples of Vs profile obtained after inversion for 4 selected locations (M05, M21, M22 and M39). The figure illustrates our two-phase approach. Phase I started with the Initial model (dotted blue line) and produced the model fitting the low frequency part of the HVSr curve (solid black line). The latter was then refined to obtain the input to phase II inversion (dashed red line). The final model was obtained after the full-frequency range inversion (yellow). Readers are encouraged to refer to the electronic color version of this paper.

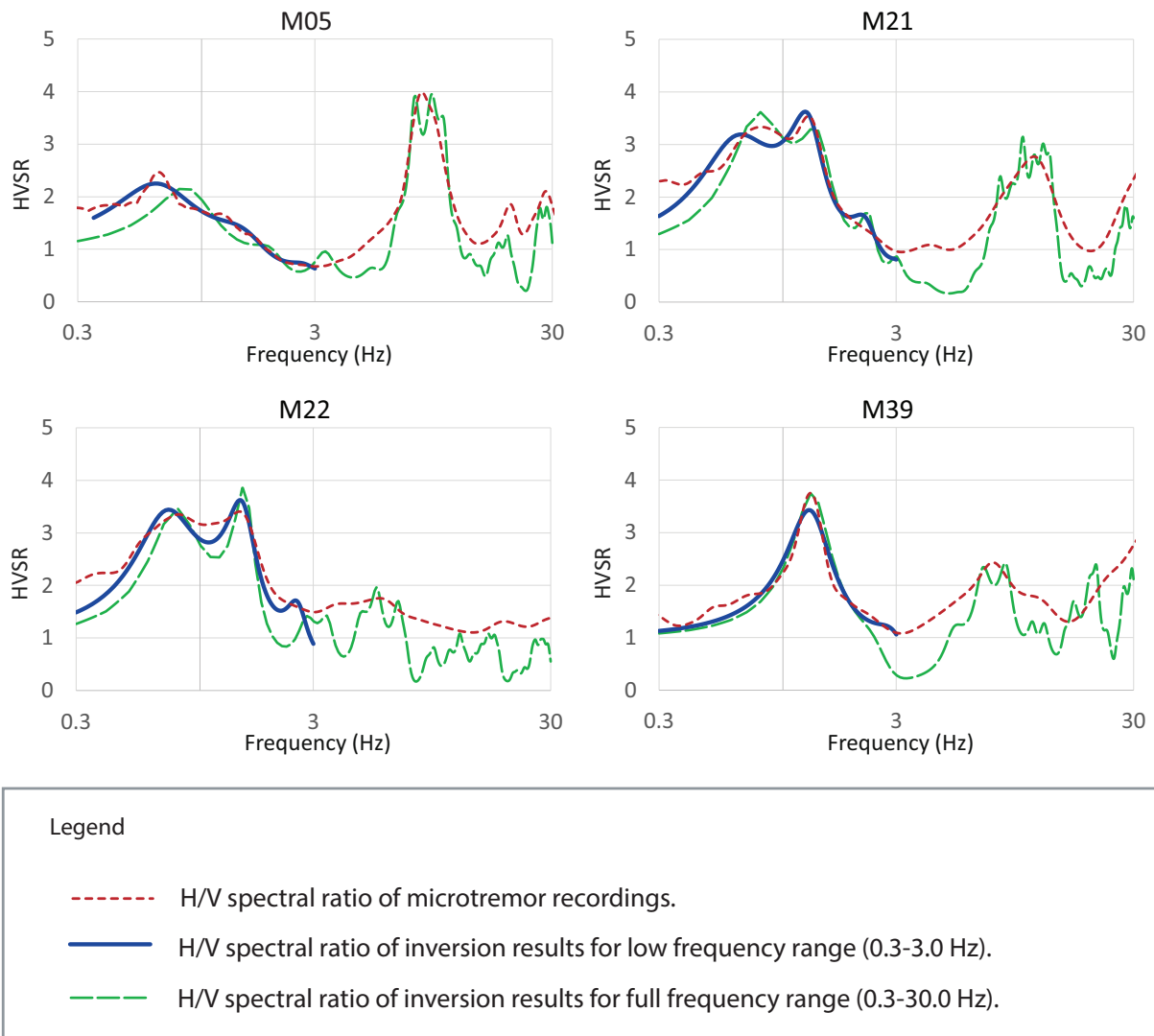


Fig. 7. The HVSR obtained for the same four selected stations M05, M21, M22 and M39 (dashed red line), along with their standard deviations (dotted grey lines) and the HVSR of the lowest misfit models for both phases of inversion (solid blue for phase I and large dashed green line for phase II). Readers are encouraged to refer to the electronic color version of this paper.

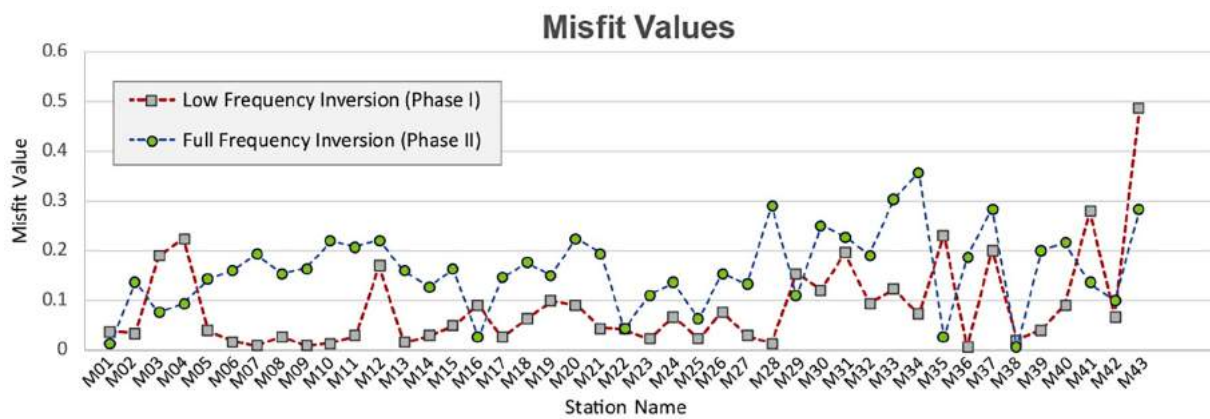
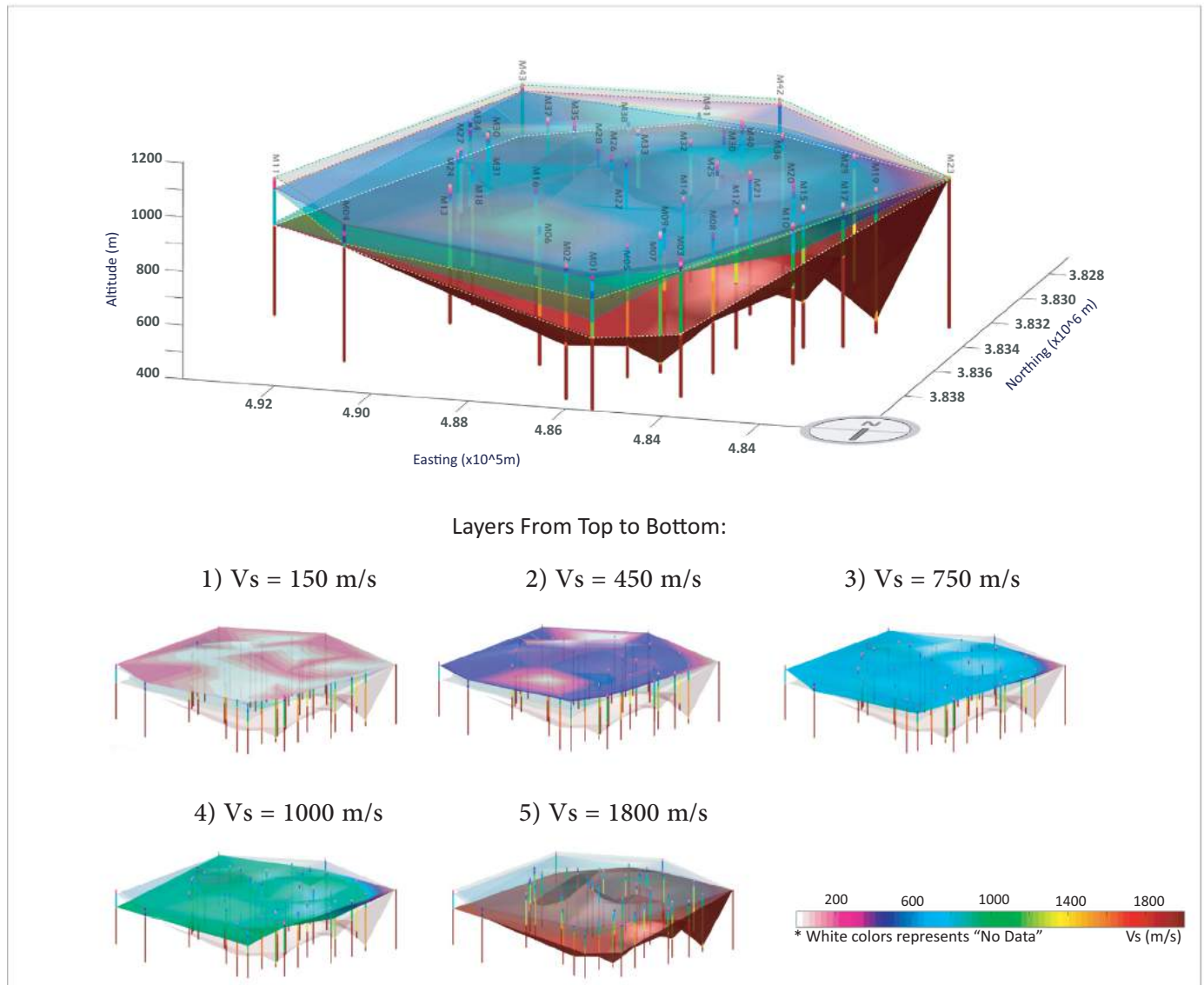


Fig. 8. Value of the normalized misfit achieved, for each station, at the end of the optimization (i.e. minimization) process. The normalized misfit ranges between 0 (target value) and 1 (initial value). Squares indicate the performance of phase I, while circles stand for phase II. These are considered as independent minimization processes.

### Shear Wave Velocity Structure of the Sediments of Qom Basin



**Fig. 9.** Three-dimensional S-wave velocity structure of Qom basin. The present result was obtained by assembling and interpolating the one-dimensional model obtained from the HVSR inversion. We extracted 5 benchmark surfaces individuating different velocities, namely 150, 450, 750, 1000 and 1800 m/s. These benchmark interfaces which are followed with the numbers 1 to 5, considered as the bottom of a sedimentary layer possessing a  $V_s$  equal or smaller to that shown in the corresponding figure label. White color represents the parts where the mentioned S-wave velocities were not applicable, i.e. the surface velocities were higher than the noted velocity.

brand new inversion. As such, the normalized misfit at the first iteration is set back to one. The second phase of inversion, because higher frequencies are considered, was more challenging. Nevertheless, the misfit values for 10 stations dropped below 0.1 and 22 stations have shown misfits between 0.1 and 0.2. Other 11 stations showed misfit values higher than 0.2 and up to 0.35. Fig. 8 shows the value of the normalized misfit value obtained for each station after convergence occurred (i.e. at the end of the optimization process). Squares indicate the performance of phase I, while circles stand for phase II.

#### 4.2. The results of the inversion analysis

In most stations, a correlation can be followed between the depth suggested by electrical resistivity and the deep-most S-wave velocity contrast in the inversion results. However, there are some stations in which such a relationship is not recognized, especially where the microtremor inversions suggest considerably thicker sediments than

electrical resistivity surveys. The final inverted 1D models for all stations have been combined to create a three-dimensional representation of the subsurface shear wave velocity distribution across the basin (Fig. 9). This figure shows five different benchmark depths (i.e. surfaces), with shear wave velocities of: 150 m/s, 450 m/s, 750 m/s, 1000 m/s and 1800 m/s, as illustrated by labels 1 to 5, respectively. These surfaces may also be viewed as the bottom boundaries of sedimentary layers (ranging from the surface, down to the benchmark), with  $V_s$  equal or lower than the corresponding benchmark's velocity. As stated earlier regarding the inversion results, the velocity structure includes discrete boundaries of sharp velocity contrasts. Therefore, to construct the 3D model of Fig. 9, every layer of every station has been divided into 1.0 m thick sublayers and a five-points moving average with five times repetition has been applied to such sublayers. In these ways, sharp velocity boundaries were slightly smoothed, creating a more realistic model and allowing to estimate the depth of the aforementioned S-wave velocity benchmarks more realistically. In the following

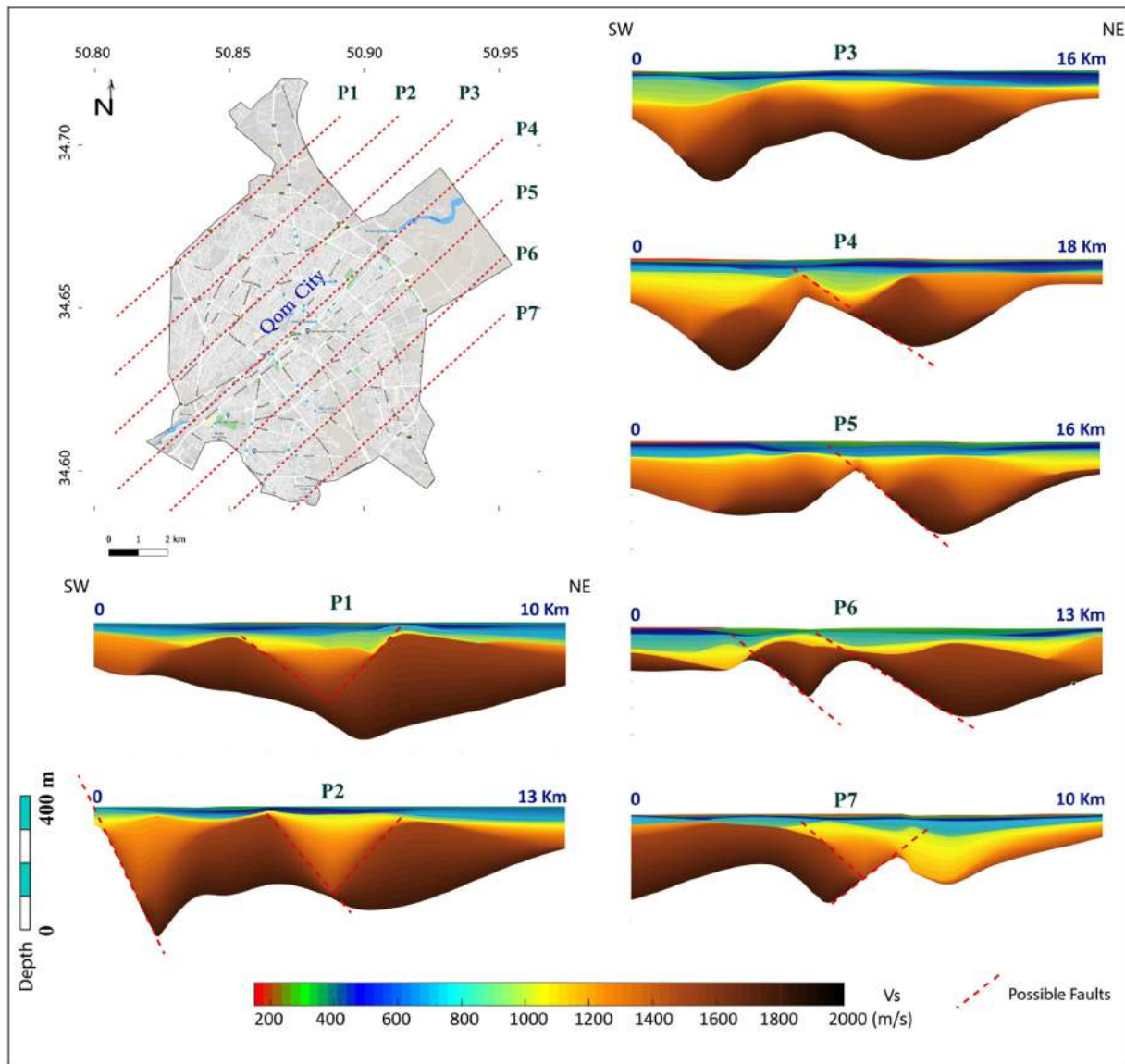


**Fig. 10.** Two dimensional NE-SW profiles of the basin structure showing the shear wave velocity distribution. Observed variations, further highlighted with dashed lines, suggest the presence of rock faults.

we describe our results and conclusions in terms of both these benchmarks and the sedimentary layers they individuate.

As it can be observed, the depth for all the S-wave velocity benchmarks is decreased in south-western parts of the city which is in agreement with the morphology of the area and also the results of both electrical resistivity and surface refraction surveys. Moving toward the central parts of the basin the alluviums grow thicker. This can also be observed in Fig. 10 which displays the two-dimensional structure of the basin for the 7 profiles with the labels P1 – P7 perpendicular to the basin elongation. In this 2D Profiles, color variations make it possible to present the spectral variations of shear wave velocity more realistic. It is obvious that the depth of the  $V_s = 150$  m/s benchmark, shown in Fig. 8, is extremely shallow (shown in red in Fig. 10). In a way that velocities lower than 200 m/s can be hardly observed in only southern parts of three profiles, P4, P5 and P6 (i.e. central profiles of the basin). Although  $V_s = 450$  m/s is more significantly contributes in the profiles, depth for sediments with this range of velocities barely reaches 40 m. In the  $V_s$  Structures obtained from inversion analysis, the maximum shear wave velocity for deepest layer does not exceed 1800 m/s for any of the outputs. Accordingly, this velocity has been considered as the deepest

benchmark of the basin, so we can cover all parts of achieved  $V_s$  profiles completely. However, as it can be noted, the major part of the basin consists of layers with velocities higher than 1000 m/s (brown spectrum). Moving toward south east (i.e. from Profile 1 toward profile 7), the maximum depth decreases from about 400 to 300 m. We individuated some sharp slopes as highlighted in Fig. 10, which may be related to the presence of faults. For profiles 6 and 7, the sharp depth reduction in southern parts is in agreement with electrical resistivity results (Fig. 3), which suggest the presence of a fault, never reported before, in that parts of the basin. Also, the trace of a bulge is evident in central parts of almost all profiles. This could be related to a deep bed-rock fault parallel to general elongation of the basin. Possible trends for this fault have been also highlighted in Fig. 10.

Sediments with velocities about 450 m/s (shown in dark blue), reach their highest depth in northern parts of profiles 3 and 4, however, these velocities can also be observed in mid-parts of Profiles 1 and 2 and also in both ends of profiles 5 and 6. For profile 7, sediments with this range of velocities are present in a low thickness almost horizontally layer from northern to southern parts of the basin. The velocities about 750 m/s (shown in light blue) gets shallower in central profiles, however, in northern end of first

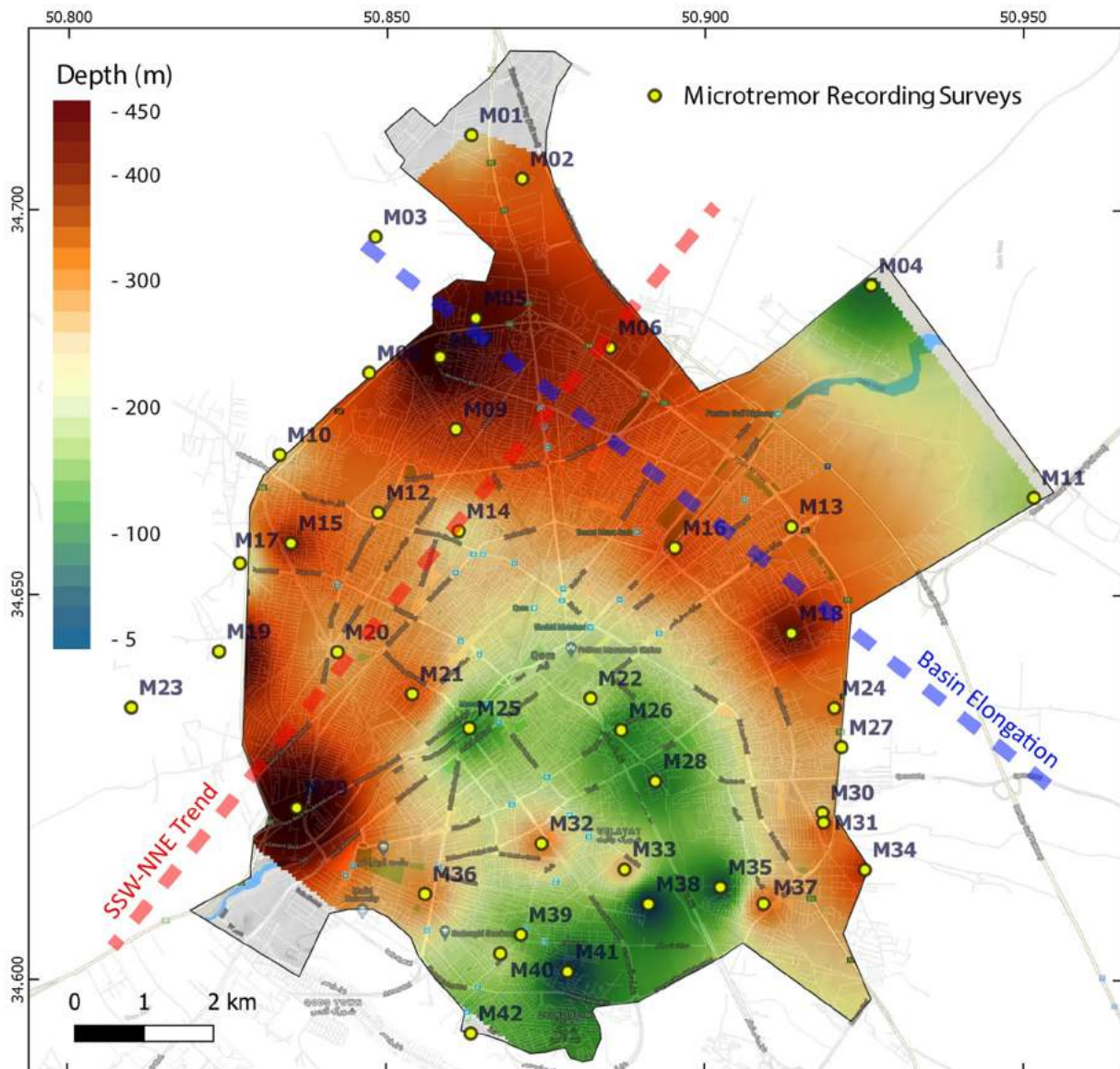


Fig. 11. Depth for the 1800 m/s shear wave velocity horizon according to microtremor inversion.

two profiles (P1 and P2) and also in central and southern parts of last two profiles (P6 and P7) their presence is considerable. Light green and yellow colors in Fig. 10 is indicative of velocities about 1000 m/s, which are varied in thickness in different parts of basin, however can considerably be observed in all profiles, most importantly, in southern end of profiles 3 and 4 and also in central and northern parts of profile 7 in which the thickness of this range of velocities exceeds 200 m.

As it is noted, the bedrock has been considered as the S-wave velocities above 1800 m/s. The contour lines corresponding to this velocity are shown in Fig. 11. In this figure, the NW-SE elongation of the basin is clearly observed (blue dash line). In the deepest parts, the depth of basin exceeds 400 m and as expected, in the north-eastern and south-western parts of the basin the depth of bedrock decreases. Another trend could also be observed in Fig. 11, with an almost SSW-NNE trend (red dash line), completely in agreement with a depression and cutting in adjacent surface topographies, which may be evidence of the less known Qomrud Fault, first described by Safaei (2009), and further investigated by Babaahmadi et al., (2010). Notably, they emphasized the importance of further studies on the Qomrud fault because

of its high activity potential. Assessing the relationship of this concavity with the mentioned fault requires further studies. Nevertheless, this seems the most credible explanation for such a feature.

As previously mentioned, the Vs30 was obtained for 34 stations by means of surface seismic refraction (Fig. 4). The Vs30 may in principle be obtained using the HVSr method as well, by averaging the top 30 m of the 1D Vs profiles produced by the inversion. Agreement between the outcomes of the two methodologies would surely improve our confidence on the overall result. Additionally, leveraging HVSr to retrieve the Vs30 would be extremely fast and cost effective. To explore this possibility, we compared these two Vs30 across the investigated area. Fig. 12 shows such comparison in terms of:

$$R_v = \frac{Vs30M - Vs30S}{Vs30S} \quad (1)$$

where Vs30M is the Vs30 according to microtremor inversions and Vs30S represents its seismic refraction surveys counterpart. This ratio ranged between 0 and more than 1 for different stations. The

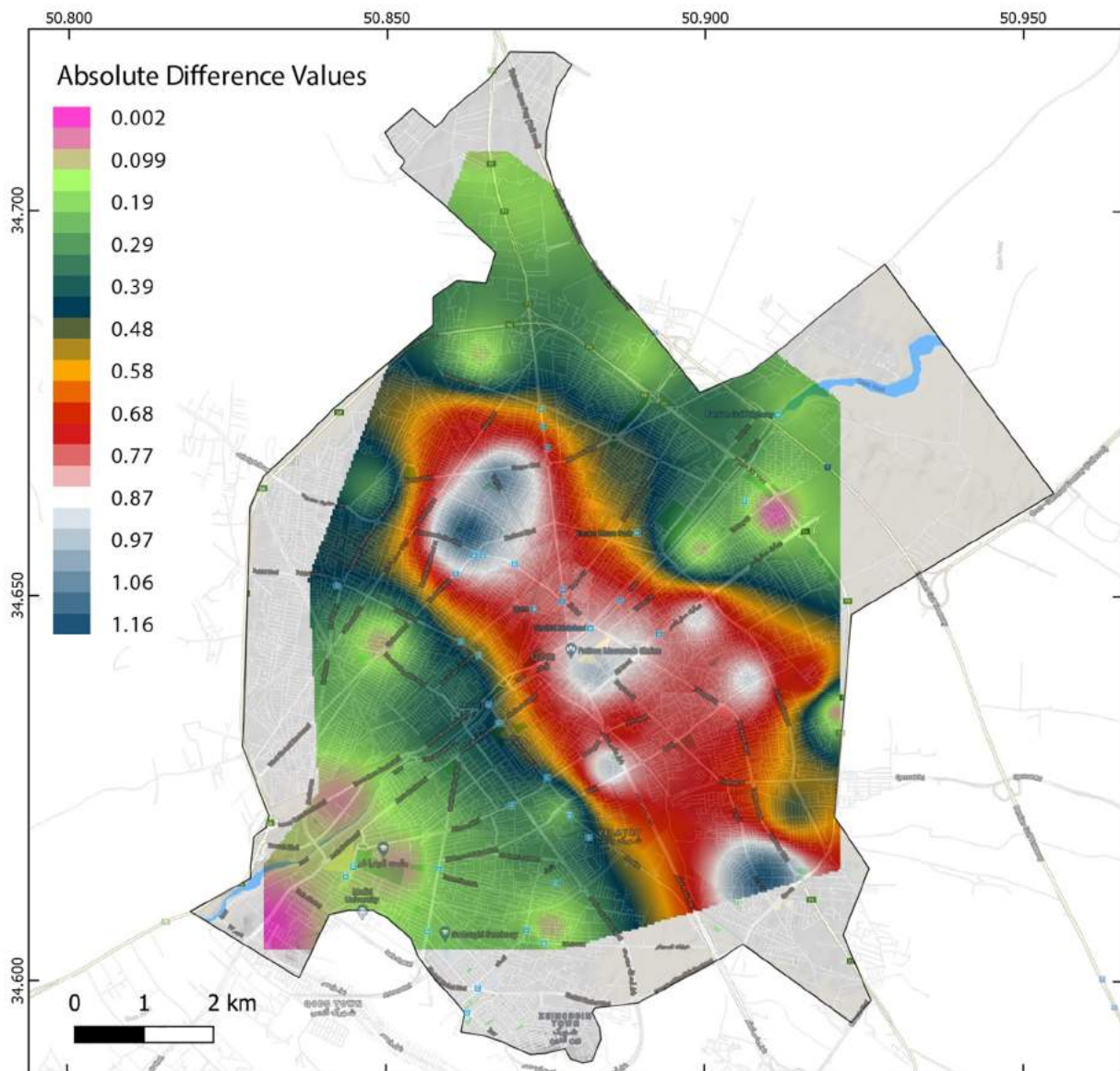


Fig. 12. The absolute S-wave velocity differences between the Vs30 from surface refraction surveys and the corresponding result estimated from microtremor inversion.

differences clearly show a trend for different parts of the basin and convey a clear message.

Despite that the microtremor inversion tries to fit the spectral ratio at all the investigated frequencies, the frequency range which is actually best fitted is around the fundamental peak. In other words, the average velocity of the full sedimentary stack is usually correctly retrieved. The shallow part of the model, mostly (but not only) impacts higher frequencies, for which unfortunately, the fit is typically difficult and less reliable. The latter phenomenon worsens as the fundamental peak sits at lower frequencies. The well-known rule  $F_0 = V_s/4H$  suggest that the Vs30 from HVSr could be expected to be reliable for very shallow bedrocks, where the Vs30 and the average velocity of the sedimentary stack are not very different. In conclusion, we expect the Vs30 to be retrieved correctly when the bedrock is sufficiently shallow. According to this explanation, we found acceptable differences (say lower than 15%), for bedrock depths smaller or around 80–100 m. Nevertheless, for deeper bedrock, where the inversion is much less sensitive to shallow velocities, the Vs30 was consistently overestimated, and even doubled in the

worst case scenarios (i.e. at the locations of deepest bedrock). Another aspect to take into account is that only 2–3 layers contributed to the computation of the Vs30 obtained from microtremors, which may be an oversimplification for the Vs30 evaluation purpose. On the one end the latter aspect may be worth further investigation. On the other hand, in our experience, when the bedrock is deep the shape of the peak and the overall curve are dominated by the average velocity of the entire stack of layers. Velocity changes in a thin shallow portion of the model barely affect such general features so that, including a multitude of thin layers within the top 30 m may reveal pointless.

Furthermore, according to the structure achieved by the microtremor inversion, the velocities for the locations where down-hole surveys were performed have been obtained. Fig. 13 compares these velocities with the results of down-hole surveys. A general agreement in depth-velocity structure can be observed. As it is noted before, in deep parts, a thick layer with the shear wave velocity of 1000 m/s can be observed for both methods. However, microtremor inversions cover significantly higher depths.

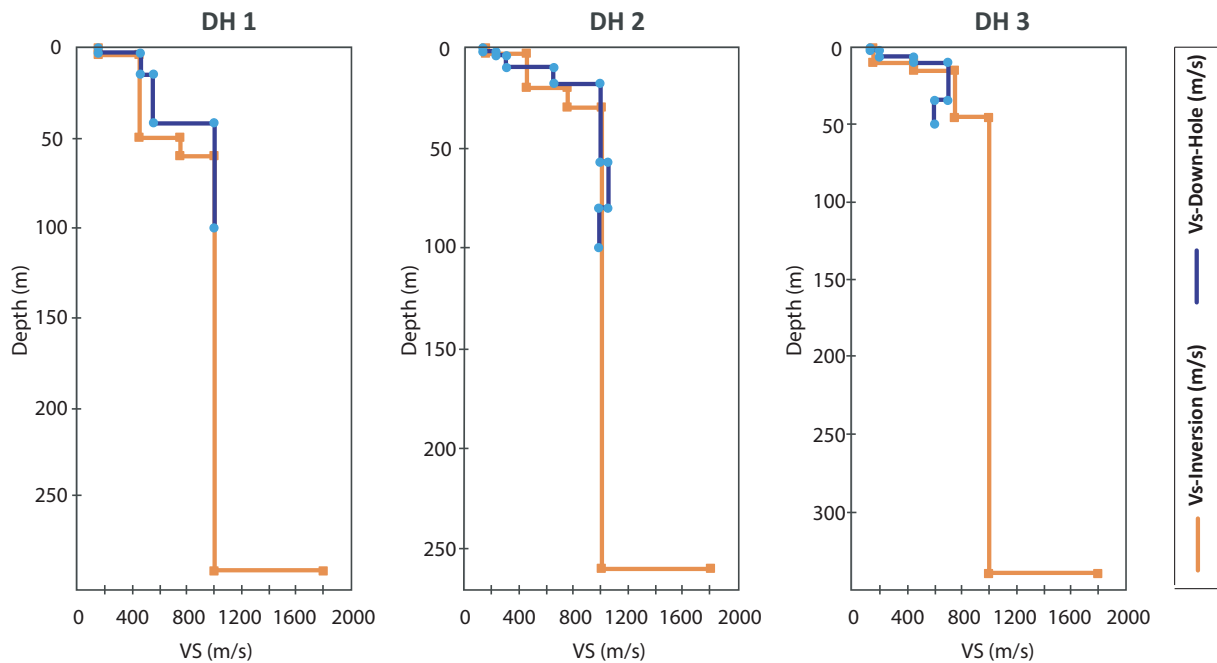


Fig. 13. Comparison of S-wave velocity structures, obtained with microtremor inversions and the results of down-hole surveys.

5. Discussion

The main contribution of the paper consists in extending the knowledge of the structure of Qom basin from the actual 30 m,

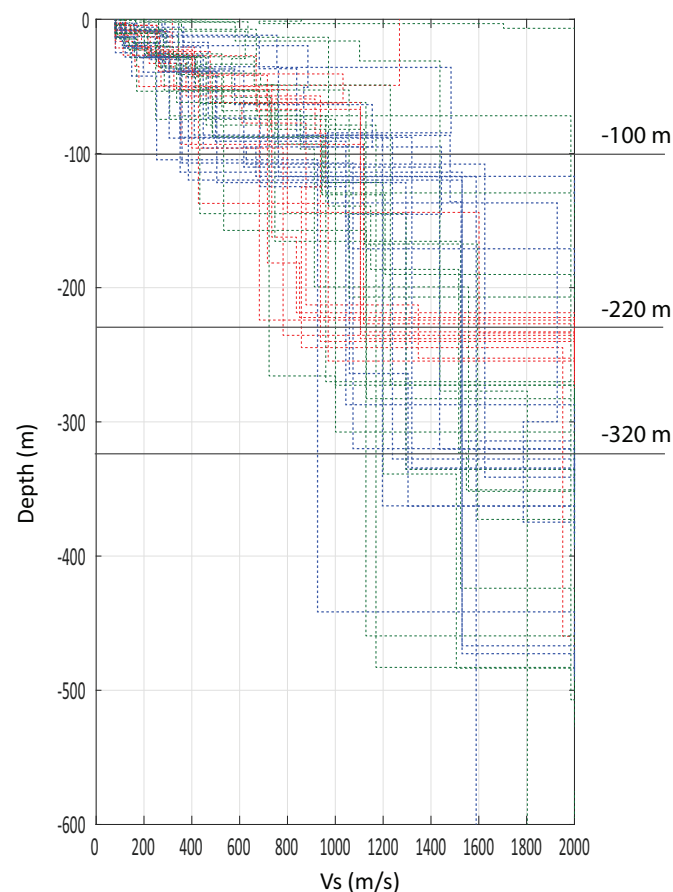


Fig. 14. A combination of Vs structures obtained for all the stations.

down to bedrock. We produced a three dimensional model of the Vs distribution which, although based on inversion of sparse HVSR measurements and therefore coarse, it provides nevertheless good evaluation of both Vs structure and bedrock's morphology.

Similar applications of HVSR can easily be found in literature. From a seismological perspective, most approaches are concerned with retrieving the local (to the site) Vs and the Vs30. HVSR is typically leveraged to this end and in connection to additional seismic methods. These approaches, abundantly referenced in the introductory section, often leverage the inversion of HVSR curves.

In contrast, sediment thickness determination does not usually require an approach as involved and sophisticated as inversion. The task is often tackled with the approach introduced by Ibs-Von Seht and Wohlenberg (1999), where the thickness (D) of the sedimentary cover is evaluated by either using an approximate local estimate of the subsurface velocity profile or alternatively, by simply determining

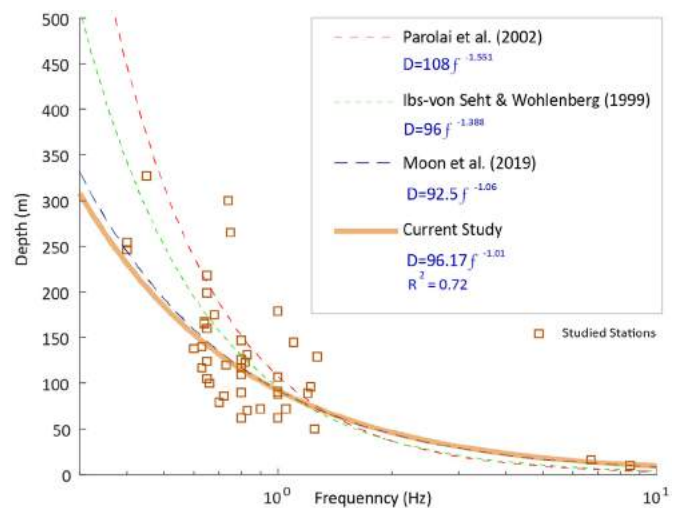


Fig. 15. Comparison between empirical depth-frequency correlations commonly found in literature (dashed lines) and a correlation computed from the results of our inversion (solid line).

the best estimation of two-parameters (a, b) for a regression law of the form

$$D = af_0^b \quad (2)$$

where  $f_0$  is the frequency associated to the curve peak identified to be the fundamental resonance and  $D$  is available for part of the measurement locations (Parolai et al. 2002; Johnson and Lane 2016; Bignardi 2017).

In principle, assuming a good estimate of the average  $V_s$  is known, the depth to bedrock could be also evaluated from the formula (Lanzo and Silvestri, 1999).

$$D = V_s/4f_0 \quad (3)$$

Nevertheless, the latter has been proved to be fairly inaccurate for realistic subsurface (Bignardi 2017). Ibs-von Seht's and Wohlenberg's formula (2) generalizes Eq. (3) to a normally varying  $V_s$  (i.e. increasing with depth), and can achieve far greater accuracy for  $D$  (error down to 5–10% of the true depth). In addition, Eq. (2) circumvents the need of a-priori knowledge of the  $V_s$  profile. However, it must be emphasized that both approaches account for only one major  $V_s$  discontinuity (i.e. bedrock), while the  $V_s$  profile is assumed either to increase with the depth or to be constant, respectively.

Fig. 14 illustrates a combination of all of  $V_s$  structures obtained through the inversion. Three major velocity contrasts can be highlighted for most of the stations, at about 100, 220 and 320 m, respectively. The set of blue profiles highlights those stations at which two characteristic contrasts are encountered, at 100 and 320 m depth.

As it can be observed the simple equation  $D = V_s/4f_0$  is not accurate in predicting the depth of these elastic impedance contrasts. Furthermore, as the increase in  $V_s$  is not necessarily smooth and comprises at least one extra impedance jump, a relationship such as (2) may reveal to be, for the present situation not accurate as the literature would suggest.

Therefore, as a final exercise, trusting that the depth-to-bedrock obtained from the inversion is realistic, we decided to use such information to verify how similar a relation (2) computed using the inversion result would compare to other literature regressions (Fig. 15). In this case we considered the bedrock as the deepest jump present velocity profiles, produced by inversion, with velocity higher than 1000 m/s. The corresponding fundamental frequency is obtained from the HVSR curves computed for the corresponding locations (Appendices 2). The computed curve shares striking similarity with other regressions, yet we know that the  $V_s$  model possesses at least two significant impedance contrasts as opposed to the smooth variation assumption. Such contrasts cannot be captured by relations such as (2) while they could be recognized by the inversion.

Finally, we must emphasize that Ibs-von Seht's and Wohlenberg's (1999) method is a viable option only when there is a sufficient number of wells reaching the bedrock as compared to the number of measurements (most applications use a measurement-wells ratio of at least 3:1). Unfortunately, no well reaching the bedrock exist for the Qom basin, which leaves inversion the only truly viable option. In this context, the capability of inverting curves from hundreds of stations simultaneously offered by the *OpenHVSR* software largely speeded up processing and the production of our tridimensional model. In this study the inversion performed on a regular PC (core i5 CPU and 12 Gb of RAM), which comprised 25,000 iterations per station, required less than 20 min.

## 6. Conclusion

In this paper, the structure of the sedimentary cover of the alluvial basin of Qom city (Iran) has been investigated using the natural seismic noise (microtremor), recorded at 43 different locations and employing the HVSR technique. The software "OpenHVSR-Inversion" has been used for the inversion of HVSR curves in order to retrieve the subsurface distribution of the elastic parameters (mainly  $V_s$ ). The parameters used to initialize the inversion have been estimated according to available geotechnical investigations, which comprised: down-hole surveys for evaluating velocity variations, electrical resistivity surveys in order to anticipate the alluvium thicknesses, and shallow boreholes which provided insight on density variations. In this paper, we aimed at constructing a structural model of the sedimentary basin in terms of shear wave velocity. In this regard,  $V_s$  structures obtained from microtremor inversion have been integrated to form both 3D and 2D representations of the sedimentary stack. The bedrock structure achieved by inversion is in a good agreement with morphology of the basin and other independent sources of information. Furthermore, analysis of these structures provided further evidences of two major faults in the area. One, the "Qomrud" fault, which has been poorly investigated so far, and a second, parallel to general elongation of the basin, never reported before. The second contribution of the paper was to investigate to what extent HVSR inversion could be used to infer the  $V_s30$  distribution. To this purpose we used the  $V_s30$  provided from previous surveys as a benchmark. Intuitively, it may be expected that such an experiment could be successful only for very shallow bedrock depths (not much deeper than 30 m), and indeed while the comparison generally showed good correlation, in the case of thin sedimentary covers, whenever microtremors could be considered to be significantly affected by deep sediments the  $V_s30$  was largely overestimated. Nevertheless, in contrast to our intuition, we must emphasize that for relatively shallow bedrock (maximum 80–100 m) the difference in  $V_s30$  from the benchmark was lower than 10–15%. However, comparing the velocities resulted by inversions by those achieved in down-hole surveys shows good correlation for deep sediments. Furthermore, we discussed the applicability of empirical relationships for estimating bed-rock depth in the investigated basin.

## Declaration of Competing Interest

The authors declare that they have no known competing financial interests or personal relationships that could have appeared to influence the work reported in this paper.

## Appendix A. Appendices

### A.1. Subsurface models achieved by microtremor inversions

### A.2. Measured and calculated HVSR curves

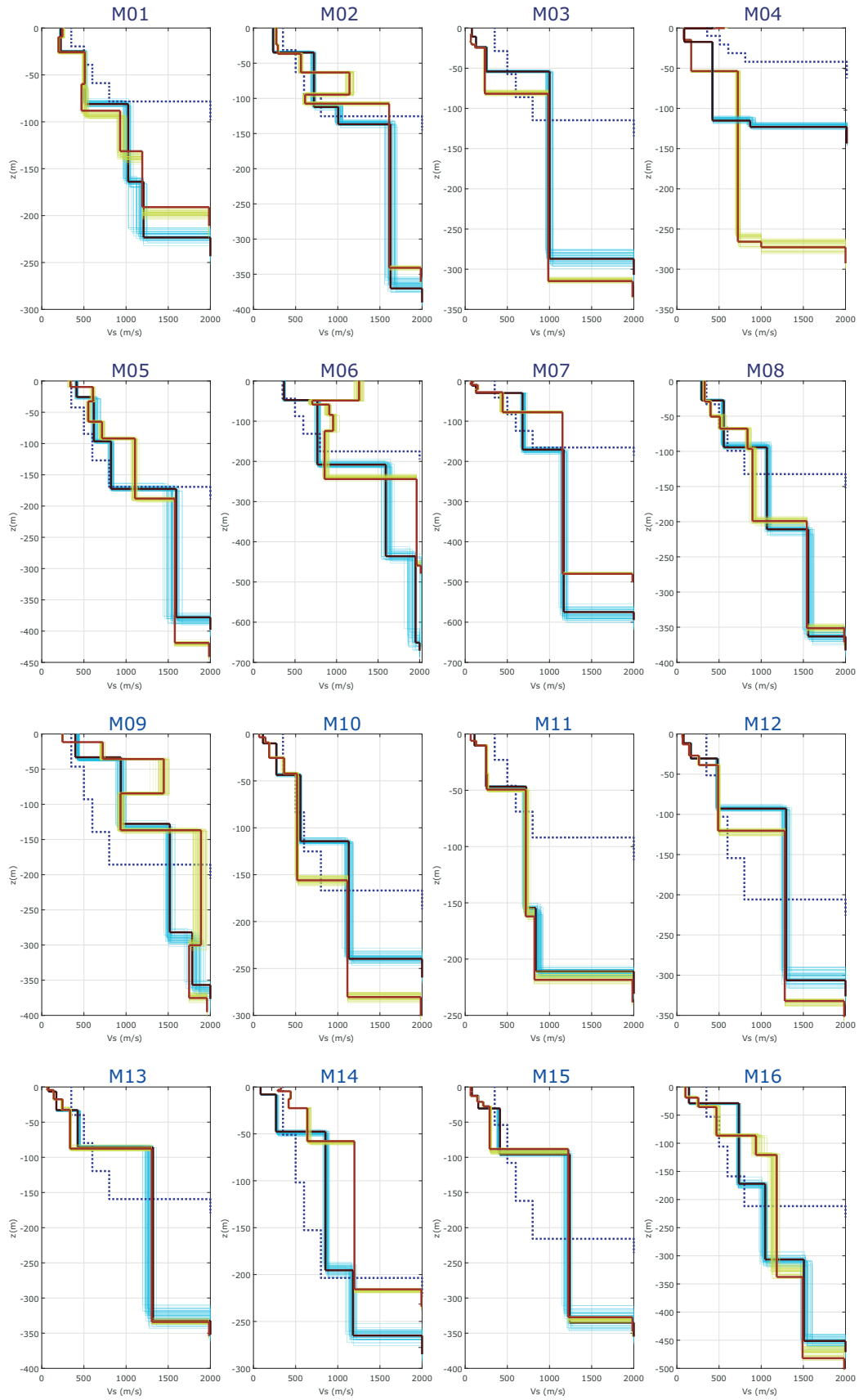


**Fig. A-1.** Fig: Vs profile obtained after inversions. The figure illustrates our two-phases approach. Phase I started with the Initial model (dotted blue line) and produced the model fitting the low frequency part of the HVSr curve (solid black line). The latter was then refined to obtain the input to phase II inversion (dashed red line). The final model was obtained after the full-frequency range inversion (yellow). Readers are encouraged to refer to the electronic color version of this paper.

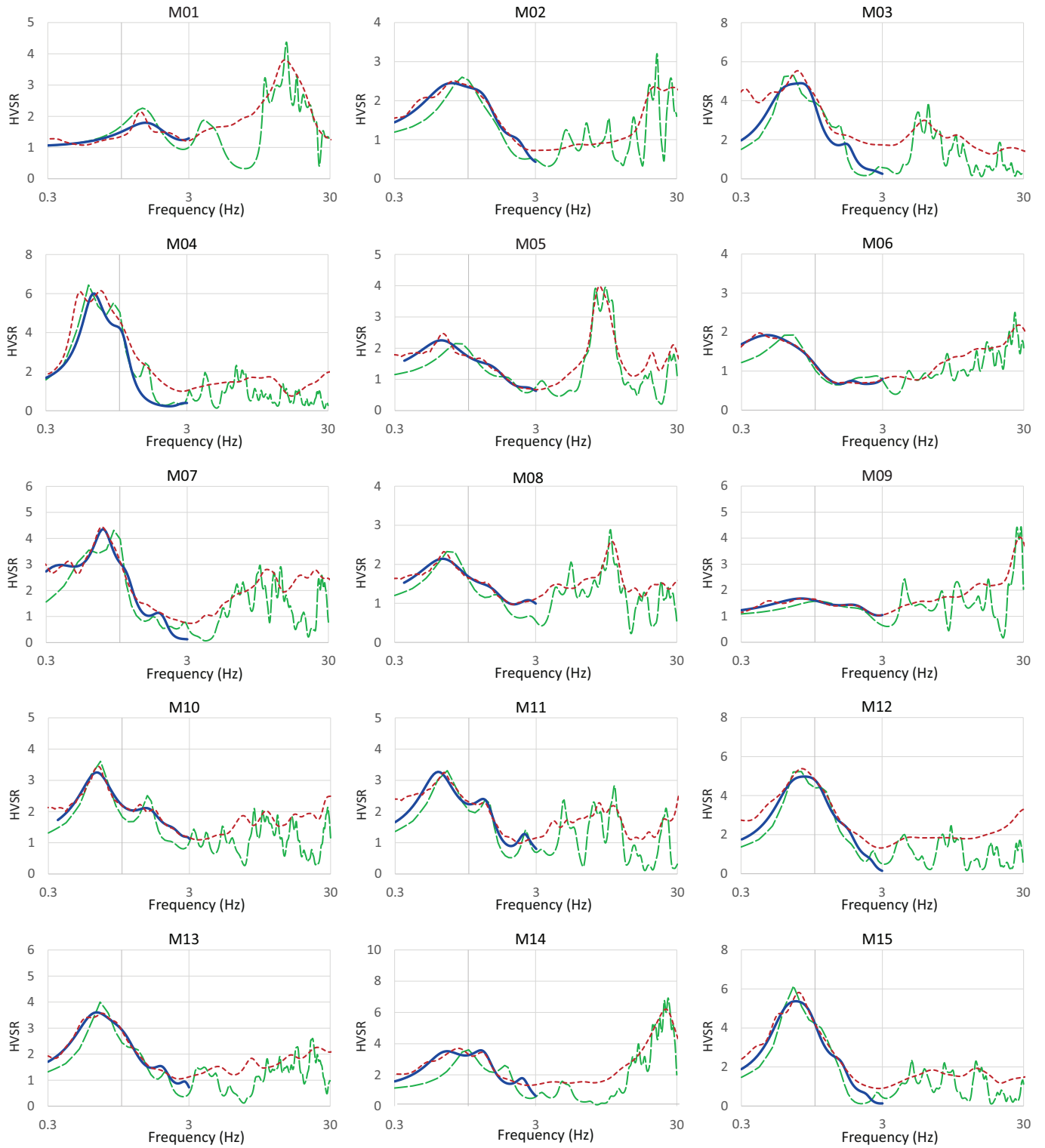


**Fig. A-2.** The HVSR obtained for the all stations (dashed red line), along with their standard deviations (dotted grey lines) and the HVSR of the lowest misfit models for both phases of inversion (solid blue for phase I and large dashed green line for phase II). Readers are encouraged to refer to the electronic color version of this paper.

## References

- Akin, Ö., Sayil, N., 2016. Site characterization using surface wave methods in the Arsin-Trabzon province, NE Turkey. *Environ. Earth Sci.* 75, 1–17. <https://doi.org/10.1007/s12665-015-4840-6>.
- Akkaya, İ., Özvan, A., 2019. Site characterization in the Van settlement (Eastern Turkey) using surface waves and HVSR microtremor methods. *J. Appl. Geophys.* 160, 157–170. <https://doi.org/10.1016/j.jappgeo.2018.11.009>.
- Albarelo, D., Castellaro, S., 2011. Tecniche sismiche passive: indagini a stazione singola. *Ing. Sismica* 38, 32–49.
- Arai, H., Tokimatsu, K., 2005. S-wave velocity profiling by joint inversion of microtremor dispersion curve and horizontal-to-vertical (H/V) spectrum. *Bull. Seismol. Soc. Am.* 95, 1766–1778. <https://doi.org/10.1785/0120040243>.
- Babaahmadi, A., Safaei, H., Yassaghi, A., Vafa, H., Naeimi, A., Madanipour, S., Ahmadi, M., 2010. A study of Quaternary structures in the Qom region, West Central Iran. *J. Geodyn.* 50, 355–367. <https://doi.org/10.1016/j.jog.2010.04.006>.
- Bekler, T., Demirci, A., Ekinci, Y.L., Büyüksarıç, A., 2019. Analysis of local site conditions through geophysical parameters at a city under earthquake threat: Çanakkale, NW Turkey. *J. Appl. Geophys.* 163, 31–39. <https://doi.org/10.1016/j.jappgeo.2019.02.009>.
- Bignardi, S., 2017. The uncertainty of estimating the thickness of soft sediments with the HVSR method: a computational point of view on weak lateral variations. *J. Appl. Geophys.* 145, 28–38. <https://doi.org/10.1016/j.jappgeo.2017.07.017>.
- Bignardi, S., Fedele, F., Santarato, G., Yezzi, A.J., Rix, G.J., 2013. Surface waves in laterally heterogeneous media. *J. Eng. Mech.* 139, 1158–1165.
- Bignardi, S., Mantovani, A., Abu Zeid, N., 2016. OpenHVSR: Imaging the subsurface 2D/3D elastic properties through multiple HVSR modeling and inversion. *Comput. Geosci.* 93, 103–113. <https://doi.org/10.1016/j.cageo.2016.05.009>.
- Bignardi, S., Zeid, N.A., Corradini, E., Santarato, G., 2017. The HVSR technique from array data, speeding up mapping of paleo-surfaces and buried remains. The case of the Bronze-Age site of Pilastris (Italy). *SEG Tech. Progr. Expand. Abstr.* 36, 5119–5124.
- Bignardi, S., Yezzi, A.J., Fiussello, S., Comelli, A., 2018. OpenHVSR - Processing toolkit: Enhanced HVSR processing of distributed microtremor measurements and spatial variation of their informative content. *Comput. Geosci.* 120, 10–20. <https://doi.org/10.1016/j.cageo.2018.07.006>.
- Bonnefoy-Claudet, S., Köhler, A., Cornou, C., Wathelet, M., Bard, P.-Y., 2008. Effects of love waves on microtremor H/V ratio. *Bull. Seismol. Soc. Am.* 98, 288–300.
- Chávez-García, F.J., Rodríguez, M., Field, E.H., Hatzfeld, D., 1997. Topographic site effects. A comparison of two nonreference methods. *Bull. Seismol. Soc. Am.* 87, 1667–1673.
- Cipta, A., Rudyanto, A., Afif, H., Robiana, R., Solikhin, A., Omang, A., Supartoyo, Hidayati S., 2020. Unearthing the buried Palu–Koro Fault and the pattern of damage caused by the 2018 Sulawesi Earthquake using HVSR inversion. *Geol. Soc. London Spec. Publ.* <https://doi.org/10.1144/sp501-2019-70>.
- Cornou, C., Chaljub, E., Tsuno, S., 2008. Real and Synthetic Ambient Noise Recordings in the Grenoble Basin: Reliability of the 3D Numerical Model Table 1: Geophysical parameters for the Grenoble basin. October.
- Fäh, D., Kind, F., Giardini, D., 2003. Inversion of local S-wave velocity structures from average H/V ratios, and their use for the estimation of site-effects. *J. Seismol.* 7, 449–467. <https://doi.org/10.1023/B:JOSE.0000005712.86058.42>.
- Gallipoli, M.R., Bianca, M., Mucciarelli, M., Parolai, S., Picozzi, M., 2013. Topographic versus stratigraphic amplification: Mismatch between code provisions and observations during the L'Aquila (Italy, 2009) sequence. *Bull. Earthq. Eng.* 11, 1325–1336. <https://doi.org/10.1007/s10518-013-9446-3>.
- Gouveia, F., Gomes, R.C., Lopes, I., 2019. Shallow and in depth seismic testing in urban environment: a case study in Lisbon Miocene stiff soils using joint inversion of active and passive Rayleigh wave measurements. *J. Appl. Geophys.* 169, 199–213. <https://doi.org/10.1016/j.jappgeo.2019.06.022>.
- Herak, M., 2008. ModelHVSR-A Matlab® tool to model horizontal-to-vertical spectral ratio of ambient noise. *Comput. Geosci.* 34, 1514–1526. <https://doi.org/10.1016/j.cageo.2007.07.009>.
- Herak, M., Allegretti, I., Herak, D., Kuk, K., Kuk, V., Maričić, K., Markušić, S., Stipčević, J., 2010. HVSR of ambient noise in Ston (Croatia): comparison with theoretical spectra and with the damage distribution after the 1996 Ston-Slano earthquake. *Bull. Earthq. Eng.* 8, 483–499.
- Ibs-Von Seht, M., Wohlenberg, J., 1999. Microtremor measurements used to map thickness of soft sediments. *Bull. Seismol. Soc. Am.* 89, 250–259.
- IIIES, 2005. International-Institute-of-Earthquake-Engineering-and-Seismology-of-Iran Final Report of Seismic and Geotechnical Microzonation of Qom City (in Persian).
- Johnson, C.D., Lane, J.W., 2016. Statistical comparison of methods for estimating sediment thickness from horizontal-to-vertical spectral ratio (HVSR) seismic methods: An example from Tylerville, Connecticut, USA. *Proceedings of the Symposium on the Application of Geophysics to Engineering and Environmental Problems*. SAGEEP.
- Kamalian, M., Kazem, M., Reza, M., 2008. Site effect microzonation of Qom, Iran. *Eng. Geol.* 97, 63–79. <https://doi.org/10.1016/j.enggeo.2007.12.006>.
- Kanai, K., Tanaka, T., Osada, K., 1954. Measurement of the microtremor. *Bull. Earthq. Res. Inst. Tokyo* 32, 199–209.
- Konno, K., Ohmachi, T., 1998. Ground-motion characteristics estimated from spectral ratio between horizontal and vertical components of microtremor. *Bull. Seismol. Soc. Am.* 88, 228–241.
- Lanzo, Giuseppe, Silvestri, Francesco, 1999. "Risposta Sismica Locale Teoria Ed Esperienze." (In Italian) Benevento: Hevelius. *Print Argomenti Di Ingegneria Geotecnica* 0010.
- Lunedei, E., Albarello, D., 2010. Theoretical HVSR curves from full wavefield modelling of ambient vibrations in a weakly dissipative layered Earth. *Geophys. J. Int.* 181, 1093–1108.
- Lunedei, E., Malischewsky, P., 2015. A Review and some New Issues on the Theory of the H/V Technique for Ambient Vibrations. *Geotech. Geol. Earthq. Eng.* 34. <https://doi.org/10.1007/978-3-319-07118-3>.
- Mahajan, A.K., Mundepi, A.K., Chauhan, N., Jasrotia, A.S., Rai, N., Gachhayat, T.K., 2012. Active seismic and passive microtremor HVSR for assessing site effects in Jammu city, NW Himalaya, India-a case study. *J. Appl. Geophys.* 77, 51–62. <https://doi.org/10.1016/j.jappgeo.2011.11.005>.
- Moon, S.W., Subramaniam, P., Zhang, Y., Vinoth, G., Ku, T., 2019. Bedrock depth evaluation using microtremor measurement: empirical guidelines at weathered granite formation in Singapore. *J. Appl. Geophys.* 171, 103866. <https://doi.org/10.1016/j.jappgeo.2019.103866>.
- Mucciarelli, M., Gallipoli, M.R., Di Giacomo, D., Di Nota, F., Nino, E., 2005. The influence of wind on measurements of seismic noise. *Geophys. J. Int.* 161, 303–308.
- Nakamura, Y., 1989. A method for dynamic characteristics estimation of subsurface using microtremor on the ground surface. *Q. Rep. Railw. Tech. Resear. Inst.*
- Nakamura, Y., 2019. What is the Nakamura Method? *Seismol. Res. Lett.* 90, 1437–1443. <https://doi.org/10.1785/0220180376>.
- Özalaybey, S., Zor, E., Ergintav, S., Tapırdamaz, M.C., 2011. Investigation of 3-D basin structures in the Izmit Bay area (Turkey) by single-station microtremor and gravimetric methods. *Geophys. J. Int.* 186, 883–894. <https://doi.org/10.1111/j.1365-246X.2011.05085.x>.
- Pamuk, E., Akgün, M., Özdağ, Ö.C., Gönenç, T., 2017. 2D soil and engineering-seismic bedrock modeling of eastern part of Izmir inner bay/Turkey. *J. Appl. Geophys.* 137, 104–117. <https://doi.org/10.1016/j.jappgeo.2016.12.016>.
- Panzera, F., Romagnoli, G., Tortorici, G., D'Amico, S., Rizza, M., Catalano, S., 2019. Integrated use of ambient vibrations and geological methods for seismic microzonation. *J. Appl. Geophys.* 170, 103820. <https://doi.org/10.1016/j.jappgeo.2019.103820>.
- Parolai, S., Bormann, P., Milkereit, C., 2002. New relationships between Vs, thickness of sediments, and resonance frequency calculated by the H/V ratio of seismic noise for the cologne area (Germany). *Bull. Seismol. Soc. Am.* 92, 2521–2527. <https://doi.org/10.1785/0120010248>.
- Pilz, M., Parolai, S., Picozzi, M., Wang, R., Leyton, F., Campos, J., Zschau, J., 2010. Shear wave velocity model of the Santiago de Chile basin derived from ambient noise measurements: a comparison of proxies for seismic site conditions and amplification. *Geophys. J. Int.* 182, 355–367. <https://doi.org/10.1111/j.1365-246X.2010.04613.x>.
- QWR, 2009. Qom-Water-Resources-Company, 2009 The final report of underground water exploration studies in Qom plain. (In Persian).
- Rahman, M.Z., Siddiqua, S., Kamal, A.S.M.M., 2016. Shear wave velocity estimation of the near-surface materials of Chittagong City, Bangladesh for seismic site characterization. *J. Appl. Geophys.* 134, 210–225. <https://doi.org/10.1016/j.jappgeo.2016.09.006>.
- Raptakis, D., Makra, K., 2010. Shear wave velocity structure in western Thessaloniki (Greece) using mainly alternative SPAC method Shear wave velocity structure in western Thessaloniki (Greece) using mainly alternative SPAC method. *Soil Dyn. Earthq. Eng.* 30, 202–214. <https://doi.org/10.1016/j.soildyn.2009.10.006>.
- Safaei, H., 2009. Study of Seismicity and Risk of Earthquakes of Khashan City, Project Number 103/9/4226, University of Isfahan, Iran. 230 pgs (in Persian).
- Sauret, E.S.G., Beaujean, J., Nguyen, F., Wildemeersch, S., Brouyere, S., 2015. Characterization of superficial deposits using electrical resistivity tomography (ERT) and horizontal-to-vertical spectral ratio (HVSR) geophysical methods: a case study. *J. Appl. Geophys.* 121, 140–148. <https://doi.org/10.1016/j.jappgeo.2015.07.012>.
- SESAME\_European\_project, Pierre-Yves BARD, 2004. Site effects assessment using ambient excitations; deliverable D23.12: guidelines for the implementation of the H/V spectral ratio technique on ambient vibrations: measurements, processing and interpretation; deliverable D23.12. Final report WP12. Project No. EVG1-CT-2000-00026 [http://sesame.geopsy.org/Papers/HV\\_User\\_Guidelines.pdf](http://sesame.geopsy.org/Papers/HV_User_Guidelines.pdf).
- Tsai, N.C., Housner, G.W., 1970. Calculation of surface motions of a layered half-space. *Bull. Seismol. Soc. Am.* 60, 1625–1651.
- Tün, M., Pekkan, E., Özel, O., Guney, Y., 2016. An investigation into the bedrock depth in the Eskisehir Quaternary Basin (Turkey) using the microtremor method. *Geophys. J. Int.* 207, 589–607. <https://doi.org/10.1093/gji/ggw294>.
- Wathelet, M., Jongmans, D., Ohrnberger, M., 2004. Surface-wave inversion using a direct search algorithm and its application to ambient vibration measurements. *Near Surf. Geophys.* 2, 211–221. <https://doi.org/10.3997/1873-0604.2004018>.
- Zor, E., Özalaybey, S., Karaaslan, A., Tapırdamaz, M.C., Erkan, B., Bay, I., 2010. Estimated from Active – Passive Array Surface Wave and Single-Station. , pp. 1603–1618. <https://doi.org/10.1111/j.1365-246X.2010.04710.x>.